Coordination Variations within Binuclear Copper Dioxygen-Derived (Hydro)Peroxo and Superoxo Species; Influences upon Thermodynamic and Electronic Properties

Pradip Kumar Hota, Anex Jose, Sanjib Panda, Eleanor Dunietz, Austin Herzog, Laurianne Wojcik, Nicolas Le Poul, Catherine Belle, Edward Solomon, Kenneth Karlin

Coordination Variations within Binuclear Copper Dioxygen-Derived (Hydro)Peroxo and Superoxo Species; Influences upon Thermodynamic and Electronic Properties

Pradip Kumar Hota,[†] Anex Jose,[‡] Sanjib Panda,[†] Eleanor M. Dunietz,[‡] Austin E. Herzog,[†] Laurianne Wojcik,[¶] Nicolas Le Poul,[¶] Catherine Belle,[§] Edward I. Solomon,*[‡#] Kenneth D. Karlin*[†]

[†] Department of Chemistry, Johns Hopkins University, Baltimore, Maryland 21218, United States

[‡] Department of Chemistry, Stanford University, Stanford, California 94305, United States

[#]Stanford Synchrotron Radiation Lightsource, SLAC National Accelerator Laboratory, Menlo Park, California 94025, United States

[¶] UMR CNRS 6521, Université de Bretagne Occidentale 6 Avenue Le Gorgeu, CS 93837, 29238 Brest Cedex 3, France

[§] Université Grenoble-Alpes, CNRS, DCM, UMR 5250, 38058 Grenoble, France

ABSTRACT: Copper ion is a versatile and ubiquitous facilitator of redox chemical and biochemical processes. These include the binding of molecular oxygen to copper(I) complexes where it undergoes stepwise reduction-protonation. A detailed understanding of thermodynamic relationships between such reduced/protonated states is key to elucidate the fundamentals of the chemical/biochemical processes involved. The dicopper(I) complex $[Cu^{I}_{2}(BPMPO^{-})]^{+}$ {BPMPO-H = 2,6-bis{[(bis(2-pyridylmethyl)amino]methyl}-4-methylphenol)} undergoes cryogenic dioxygen addition; further manipulations in 2-methyltetrahydrofuran generate dicopper(II) peroxo $[Cu^{II}_{2}(BPMPO^{-})(O_2^{2-})]^{1+}$, hydroperoxo $[Cu^{II}_{2}(BPMPO^{-})(^{-}OOH)]^{2+}$ and superoxo $[Cu^{II}_{2}(BPMPO^{-})(O_2^{\cdot-})]^{2+}$ species, characterized by UV-vis, resonance Raman and EPR spectroscopies and CSI-MS. An unexpected EPR spectrum for $[Cu^{II}_{2}(BPMPO^{-})(O_2^{\cdot-})]^{2+}$ is explained by analysis of its exchange-coupled three-spin frustrated system and DFT calculations. A redox equilibrium, $[Cu^{II}_{2}(BPMPO^{-})(O_2^{2-})]^{1+} \rightleftarrows [Cu^{II}_{2}(BPMPO^{-})(O_2^{\cdot-})]^{2+}$, is established utilizing $Me_8Fc^+/Cr(\eta^6-C_6H_6)_2$, allowing for $[Cu^{II}_{2}(BPMPO^{-})(O_2^{\cdot-})]^{2+}/[Cu^{II}_{2}(BPMPO^{-})(O_2^{2-})]^{1+}$ reduction potential calculation, $E^{\circ\prime}$ = −0.44 V ± 0.01 vs $Fc^{+/o}$, also confirmed by cryoelectrochemical measurements ($E^{\circ\prime}$ = −0.40 V ± 0.01). 2,6-Lutidinium triflate addition to $[Cu^{II}_{2}(BPMPO^{-})(O_2^{2-})]^{1+}$ produces $[Cu^{II}_{2}(BPMPO^{-})(^{-}OOH)]^{2+}$; using a phosphazene base an acid–base equilibrium was achieved, pK_a = 22.3 ± 0.7 for $[Cu^{II}_{2}(BPMPO^{-})(^{-}OOH)]^{2+}$. The $BDFE_{OO-H}$ = 80.3 ± 1.2 kcal/mol, as calculated for $[Cu^{II}_{2}(BPMPO^{-})(^{-}OOH)]^{2+}$; this is further substantiated by H-atom abstraction from O–H substrates by $[Cu^{II}_{2}(BPMPO^{-})(O_2^{\cdot-})]^{2+}$ forming $[Cu^{II}_{2}(BPMPO^{-})(^{-}OOH)]^{2+}$. In comparison to known analogues, the thermodynamic and spectroscopic properties of $Cu^{II}_{2}(BPMPO^{-})$ O_2-derived adducts can be accounted for based on chelate ring size variations built into the BPMPO^{-} framework and resulting enhanced Cu^{II}-ion Lewis Acidity.

INTRODUCTION

The reactivity of copper complexes with dioxygen (O_2) is of considerable contemporary interest with respect to obtaining a full understanding of the inherent oxidative properties and capabilities of copper ions and copper-ligand complexes. Applications include utilization for battery and fuel cell technologies (i.e., the O_2 reduction reaction (ORR) to give H_2O_2 or water,[1] or use in the practical oxidation of organic substrates).[2][3][4][5] In addition, copper(I)–dioxygen adducts are important in the reaction mechanism of many copper-based metalloenzymes that process molecular oxygen.[6] These enzymes are involved in numerous biological functions including dioxygen transport, monooxygenation of substrates; one atom of O_2 is inserted into a C–H bond with the other reduced to water, or oxidase activity where the full four-electron four-proton reduction of O_2 to water is coupled to four

(4) one-electron substrate oxidations. Another type of oxidase activity involves copper-dioxygen derived species for in substrate dehydrogenation, in the oxidation of alcohols to aldehydes (e.g., galactose oxidase), or primary amine oxidative deamination yielding an aldehyde plus ammonium ion (in amine oxidases); in both of these cases the final O_2-derived product is H_2O_2.[7]

In particular and as the topic of investigation provided in this report, the role of binuclear copper (i.e., dicopper) centers is pertinent in biology. Hemocyanins (Hc), molluskan or arthropodal hemolymph O_2-transporters; reversible O_2-addition at a dicopper(I) active site produces a peroxo (O_2^{2-}) dicopper(II) center.[6,8] The dioxygen binding occurs in a μ-η^2-η^2 side-on fashion (Scheme 1). Tyrosinases (Ty)[6] are widely distributed (i.e., bacteria, fungi, plants, insects and

Scheme 1. O$_2$-Binding in Hc, Ty
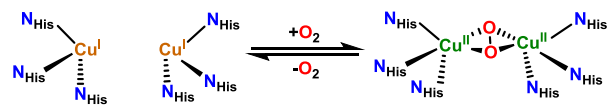
mammals) and through O₂-binding analogous to that in Hc's, *o*-hydroxylation of phenols occurs, followed by dehydrogenation of the resulting *o*-catechols, the key steps in melanin pigment biosynthesis and the well-known browning reaction observed in damaged fruits and vegetables.[9] Catechol oxidases effect just the dehydrogenation of *o*-catechols giving *o*-quinones.[6] A related enzyme, NspF, performs the four-electron oxidation of natural products possessing arylamine functionalities, giving aryl-nitroso products.[10]

The 1980's brought on a considerable research effort toward elucidation of the reaction of reduced mono- or binuclear copper centers with O₂.[11] Such coordination chemistry studies aimed to elucidate fundamentals, determine the nature of products formed, the kinetics of their formation, analysis of their spectroscopic properties and bonding as well as an elaboration of the scope and mechanism of reactions with organic substrates or protons and/or electron sources. For single copper centers, the reaction of a ligand-copper(I) complex with O₂ forms η^2-superoxo (side-on),[12] η^2-peroxo[13] or η^1-superoxo (end-on) species (not shown).[14]
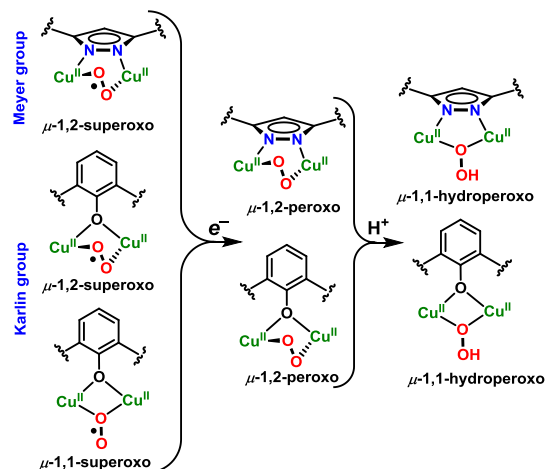

Figure 1. Dicopper(I)-dioxygen binding motifs studied using pyrazolato (Meyer group) and phenolato (Karlin group) bridging ligands (left) and after one-electron process and protonation (right).

Figure 1 illustrates what is generally known about such synthetic ligand-copper(I) complexes reacted with O₂ to give binuclear products, those from the Meyer research group employing a bridging pyrazolato ligand with pendant N_3 triazacyclononane chelates,[15 16 17] or as reported by Karlin *et al.* a central phenolato bridging ligand with pendant bis(2-(2-pyridyl)ethylamine tridentate ligands (XYLO⁻ ligand).[18 19 20] The O₂-derived products are either one-electron reduced (O₂·⁻ superoxo species, with mixtures of μ-1,2- and μ-1,1-superoxo ligands in phenolato bridged systems)[20-21] or peroxo (O₂²⁻) complexes. F. Meyer

and coworkers[17b] recently described X-ray structures of a μ-1,2-peroxo/superoxo dicopper(II) complex *pair* with a pyrazolate bridging group. The pair reversibly interconvert via one-electron redox processes occurring with a low reorganization energy (λ), also observed with a phenolato-bridged dicopper complex system.[21b] With either the pyrazolato[16c,17a] or phenolato[18e,20,22] bridging assemblies (Figure 1), protonation or other synthetic procedures allow for formation of the μ-1,1-hydroperoxo complexes.

Together with the reports discussed above, meticulous research efforts by Karlin *et al.* and Meyer *et al.* involving binuclear complexes with bridging reduced dioxygen species (O₂·⁻, O₂²⁻, ⁻OOH; Figure 1) has led to significant advances in understanding the geometric and electronic structures of this class of complexes, establishing fundamental thermodynamic relationships between these species.[17a,20] Parameters elucidated include hydroperoxo/peroxo complexes' pKa, the superoxo/peroxo reduction potential ($E^{o'}$) and from "thermodynamic square scheme" (Scheme 2) analyses, hydroperoxo complex ⁻OO–H Bond Dissociation Free Energy (BDFE).[23] Such analyses and derived data are scarce. From Mayer and coworkers,[23a] such data for "square schemes" are important in investigating mechanistic pathways for H-transfers (H⁺/e⁻) which are relevant to many chemical and biochemical processes including those with energy implications. Elucidation of the microscopic steps details (electron transfer ($E^{o'}$), proton transfer (pK_a), H• transfer, i.e., BDFE) is key for understanding the "square scheme". These parameters thus reflect on the ability of the superoxo-dicopper(II) complexes to effect substrate hydrogen atom abstraction (HAA) reactions leading to corresponding hydroperoxo dicopper(II) complexes (the diagonal approach; Scheme 2) formation. As discussed below, the particular nature of the binucleating ligand influences the thermodynamics involved.

Scheme 2. Thermodynamic Square Scheme Relevant to the Interconversion of Copper-Dioxygen Adducts. Horizontal Processes Refer to Electron Transfer (ET) whereas Vertical Routes Provide Proton Transfers (PT); the BDFE Derives from the Diagonal Process; X Represents a Bridging Ligand/Group
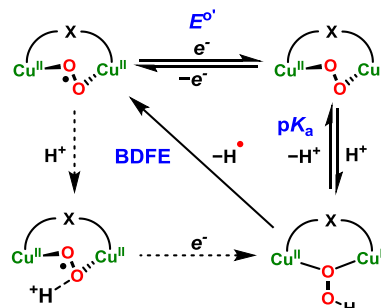
This report focuses on the reactivity and thermodynamic interrelationships of a new dicopper(I)–dioxygen complex employing a "classic" binucleating ligand which possesses a central phenolato bridge called H-BPMP and BPMPO⁻ (deprotonated; phenolate); we name this phenol

as BPMPOH (Chart 1, **A**). It comes from the era of binucleating ligands reported in 1970, first by R. Robson[24] and then S. Kida/H. Okawa.[25] In particular, H–BPMP (i.e., BPMPOH), first reported in 1981 by Suzuki and coworkers, was utilized to generate a dicobalt(II)/O_2 adduct,[26] then structurally characterized as a peroxo-dicobalt(III) complex.[27] H–BPMP has elicited wide application to binuclear complexes of copper,[28] iron,[29] cobalt,[26-27,30] manganese,[31] zinc[32] and heterobimetallic complexes.[33] $[Cu^{II}_2(BPMPO^-)(OH)]^{2+}$ and $[Cu^{II}_2(BPMPO^-)(OAc)_2]^+$,[28e,34] with phenolate and hydroxide or acetate bridges, exhibit catecholase activity with O_2 present (catechols →quinones). $[Cu^{II}_2(BPMPO^-)(H_2O)_2]^{3+}$ is also known.[28e] Réglier and Belle have reported phenylthiourea (PTU) and phenylmethylene thiosemicarbazone (PTSC) coordinated dicopper complexes of the H–BPMP ligand, as models of inhibited forms of tyrosinase.[35]

Chart 1. Binucleating Ligands, H-BPMP ($\equiv$ BPMPOH; this work) and XYLOH

H-BPMP ≡ BPMPOH

XYLOH
Previously studied

$[Cu^{II}_2(BPMPO^-)(O_2^{\cdot-})]^{2+}$

$[Cu^{II}_2(BPMPO^-)(O_2^{2-})]^{1+}$

$[Cu^{II}_2(BPMPO^-)(^-OOH)]^{2+}$
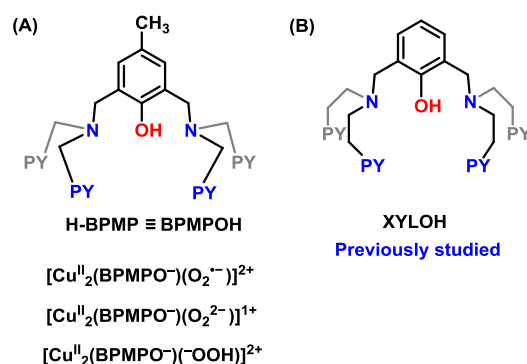
With the similarity in overall architecture of BPMPOH with the other phenol binucleating ligands, especially the previously reported XYLOH (Chart 1; **B**), we explored its dioxygen chemistry utilizing a dicopper BPMPO$^-$ framework in comparison to the previously reported XYLO$^-$ chemistry. The binucleating ligand wings of both BPMPO$^-$ and XYLO$^-$ dicopper(II) complexes possess a tridentate with two pyridyl and one alkylamino donor (Chart 1). However, the number of methylene groups in between the pyridyl functionality and the alkylamino atom differs; in XYLO$^-$ complexes, the copper ion binding to this tridentate site is supported by two six-membered chelate rings, –N-[CH_2-CH_2-(2-pyridyl)]$_2$, whereas in BPMPO$^-$, five-membered chelate rings within –N-[CH_2-(2-pyridyl)]$_2$ groups, would be present. It is known that such differences can lead to variable structural/coordination and physical property effects. These include altered ligand-Cu^{II}/ligand-Cu^I reduction potential with the five-membered rings shifting corresponding $E^{\circ\prime}$ (or $E\frac{1}{2}$) to measurably more negative values.[36] As discussed below, this latter behavior allows one to conclude that Lewis acidity of metal ion differs in a significant manner in complexes of BPMPO$^-$ vs XYLO$^-$.

RESULTS AND DISCUSSION

Phenolato–dicopper(I) $[Cu^I_2(BPMPO^-)](B(C_6F_5)_4)$, Peroxo-dicopper(II), $[Cu^{II}_2(BPMPO^-)(O_2^{2-})](B(C_6F_5)_4)$ and Hydroperoxo–dicopper(II), $[Cu^{II}_2(BPMPO^-)(^-OOH)](B(C_6F_5)_4)_2$ Complexes The binucleating ligand BPMPOH was synthesized as previously described,[28e] and isolation of the phenolato–dicopper(I) complex was achieved by ligand deprotonation using P$_1$-^{t}Bu-tris(tetramethylene) (^{t}BuP$_1$(pyrr)), followed by the addition of 2 equiv. $[Cu^I(CH_3CN)_4][BArF]$ (BArF $\equiv$ B(C_6F_5)$_4$) in MeTHF at room temperature (Scheme 3). The phenolato-bridged dicopper(I) complex $[Cu^I_2(BPMPO^-)](B(C_6F_5)_4)$ was isolated as a bright yellow solid and its formulation confirmed by Electrospray Ionization Mass Spectrometry (ESI-MS) and elemental analysis.[37] When a yellow MeTHF solution of $[Cu^I_2(BPMPO^-)]^{1+}$ is exposed to dry O_2 at –90 °C, an intense purple color develops due to the formation of the peroxo dicopper(II) complex $[Cu^{II}_2(BPMPO^-)(O_2^{2-})]^{1+}$, (Scheme 3). Its visible absorption spectrum (Figure 2A, purple line) at –90 °C exhibits its strongest transition at 536 nm (ε = 8,500 M^{-1} cm^{-1}). In addition, a band at 420 nm is observed along with an absorption in the d–d region near 620 nm. This peroxide dicopper(II) complex is EPR-silent (perpendicular mode), presumed to be due to antiferromagnetic coupling between the two copper(II) ions, a common property of dicopper(II) complexes bridged by a phenolato group.[20] The UV-vis and EPR properties are closely aligned with those observed for $[Cu^{II}_2(XYLO^-)(O_2^{2-})]^{1+}$. Cold spray ionization mass spectrometry (CSI-MS) analysis of the purple reaction mixture at –90 °C supports our formulation of this complex as $[Cu^{II}_2(BPMPO^-)(O_2^{2-})]^{1+}$ with a signal at a mass-to-charge ratio (m/z) of 687.1 for $[Cu^{II}_2(BPMPO^-)(O_2^{2-})]^{1+}$ (calculated m/z 687.1) (Figure 2B). A simulated (theoretical) MS spectrum (Figure S7) agrees, notably exhibiting the isotope pattern expected for a dicopper-containing compound dominated by ^{63}Cu and ^{65}Cu.

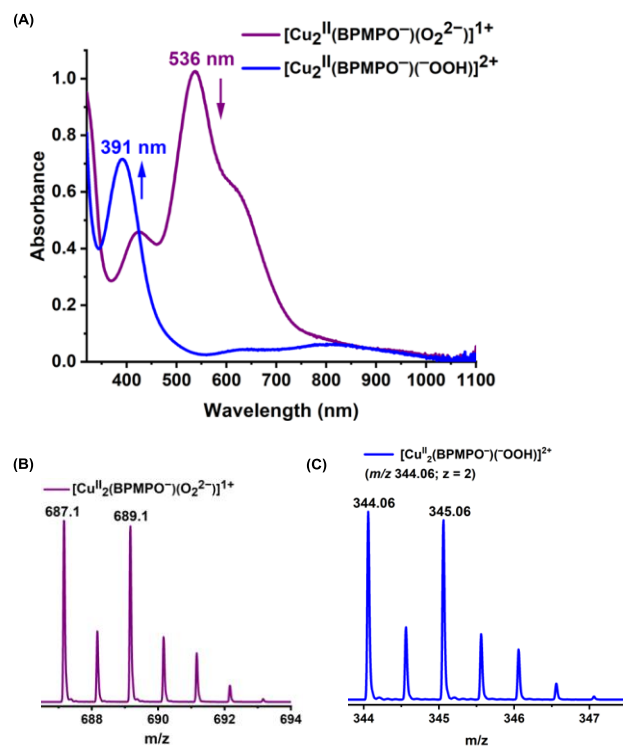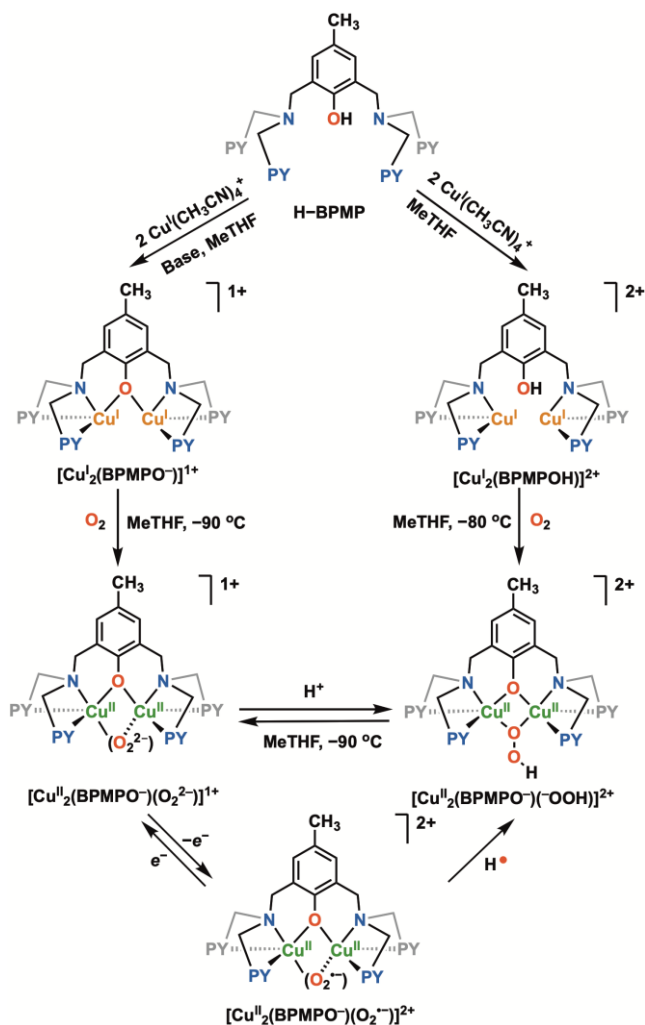**Scheme 3. Synthetic Routes for the Dioxygen Derived Binuclear Copper Complexes.**

Figure 2. (A) UV–vis spectra illustrating the conversion of $[Cu^{II}_2(BPMPO^-)(O_2^{2-})]^{1+}$ (purple) to form $[Cu^{II}_2(BPMPO^-)(^-OOH)]^{2+}$ (blue) by addition of $[(LutH^+)](OTf)$ in MeTHF at −90 °C. Dicopper(I) complex concentrations used for the UV-vis spectra were 0.125 mM. (B) CSI-MS data for $[Cu^{II}_2(BPMPO^-)(O_2^{2-})]^{1+}$. (C) CSI-MS data for $[Cu^{II}_2(BPMPO^-)(^-OOH)]^{2+}$. Simulated spectra are given in the Supporting Information.

The addition of 1 equiv. 2, 6-lutidinium triflate $[(LutH^+)](OTf)$ to the solution of $[Cu^{II}_2(BPMPO^-)(O_2^{2-})]^{1+}$ at −90 °C in MeTHF leads to peroxide protonation and formation of a corresponding hydroperoxide species, $[Cu^{II}_2(BPMPO^-)(^-OOH)]^{2+}$ (Scheme 3 and Figure 2, blue line). UV–vis spectroscopy at −90 °C of complex $[Cu^{II}_2(BPMPO^-)(^-OOH)]^{2+}$ revealed a principal band at 391 nm (ε = 5,800 M^{-1} cm^{-1}), along with less intense 630, and 800 nm bands (Figure 2). As for peroxo-dicopper(II) complex $[Cu^{II}_2(BPMPO^-)(^-OOH)]^{2+}$ this is also EPR-silent (perpendicular mode), certainly due to antiferromagnetic coupling between the two copper(II) ions. Mass spectrometry of the green reaction mixture at −90 °C supports formation of $[Cu^{II}_2(BPMPO^-)(^-OOH)]^{2+}$, with a signal at a mass-to-charge ratio (m/z) of 344.1 (z = 2) (Figure 2B) for $[Cu^{II}_2(BPMPO^-)(^-OOH)]^{2+}$, [calculated ($m/z$) of 344.0 (z = 2)]. Two additional protocols were utilized to generate the hydroperoxo complex: (1) When previously known hydroxide bridged complex with BPMPO$^-$, $[Cu^{II}_2(BPMPO^-)(^-OH)](ClO_4)_2$,[28e] was treated with 6 equiv. $H_2O_{2(aq)}$ in CH_3CN solvent at −43 °C, $[Cu^{II}_2(BPMPO^-)(^-OOH)]^{2+}$ is generated *in situ* and its formation is confirmed by ESI-MS (m/z = 786.8) (Figure S4)[37] and rR spectroscopy,

(v(O–O) = 894 cm^{-1} (λ_{exc} = 457 nm)($\Delta^{18}O_2$ = –48 cm^{-1})).[37] (2) [Cu$^{II}_2$(BPMPO$^-$)($^-$OOH)]$^{2+}$ can also be generated from the direct oxygenation of [Cu$^I_2$(BPMPOH)]$^{2+}$ (–80 °C; MeTHF), a dicopper(I) complex possessing an internal phenol, that isolated from the reaction of ligand BPMPOH with 2 equiv. [Cu^I(CH$_3$CN)$_4$][BArF] in MeTHF at room temperature (Scheme 3). This method, while proven to work well for hydroperoxo-dicopper(II) complexes derived from XYL-OH (Chart 1)[18e] or other phenol-containing binucleating ligands[22b] here led to absorptivities indicating ~ 80% of the conversion as those formed from [(LutH$^+$)](OTf) treatment of [Cu$^{II}_2$(BPMPO$^-$)(O$_2^{2-}$)]$^{1+}$ (vide supra), and so this method was not used for further studies.

Generation and Characterization of Superoxide–dicopper(II) Complex, [Cu$^{II}_2$(BPMPO$^-$)(O$_2^{\bullet-}$)]$^{2+}$. In accordance with previous reports, the superoxide–dicopper(II) complex is formed via the addition of chemical oxidants, such as ferrocenium derivatives, to the peroxo–dicopper(II) complex.[20] Addition of 1 equiv. of ferrocenium salt ((η^5-C$_5$H$_5$)$_2$FeBArF $\equiv$ FcBArF) to [Cu$^{II}_2$(BPMPO$^-$)(O$_2^{2-}$)]$^{1+}$ at –90 °C resulted in the conversion of [Cu$^{II}_2$(BPMPO$^-$)(O$_2^{2-}$)]$^{1+}$ to [Cu$^{II}_2$(BPMPO$^-$)(O$_2^{\bullet-}$)]$^{2+}$ (Scheme 3 and Figure 3). The reaction was monitored by UV–vis spectroscopy, wherein the λ_{max} = 536 nm (Figure 2) corresponding to the peroxo–dicopper(II) complex disappears and a new band at 405 nm (ε = 15,100 M^{-1} cm^{-1}) (Figure 3; green line), corresponding to the superoxo–dicopper(II) complex [Cu$^{II}_2$(BPMPO$^-$)(O$_2^{\bullet-}$)]$^{2+}$, appears. This superoxo–dicopper(II) complex is stable at cryogenic temperatures up to –80 °C; however, it thermally decays to the hydroxo–bridged complex [Cu$^{II}_2$(BPMPO$^-$)($^-$OH)]$^{2+}$ (Figure S1).[37]
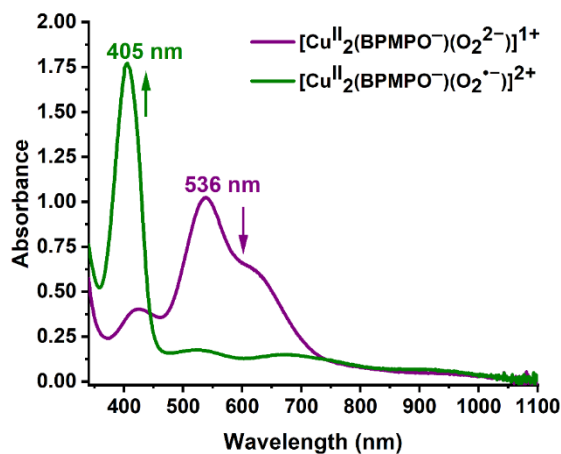
Figure 3. UV–vis spectra demonstrating the oxidation of [Cu$^{II}_2$(BPMPO$^-$)(O$_2^{2-}$)]$^{1+}$ (purple) to form [Cu$^{II}_2$(BPMPO$^-$)(O$_2^{\bullet-}$)]$^{2+}$ (green) in MeTHF at –90 °C using FcBArF.

Resonance Raman Spectroscopy. Further evidence confirming the formation of binuclear copper-dioxygen derived adducts comes from resonance Raman (rR) spectroscopy (Figure 4). The UV-vis spectra for all of these species closely mirror those known for previously well-characterized dicopper(II) complex analogs, i.e., those with the XYLO$^-$ binucleating ligand along with and other phenolato-bridged complexes (UNO$^-$ and PD'O$^-$; Figure 5),[21b,22b] allowing us to readily home in on desirable excitation wavelengths for use in rR spectroscopy on frozen MeTHF solutions of these samples.
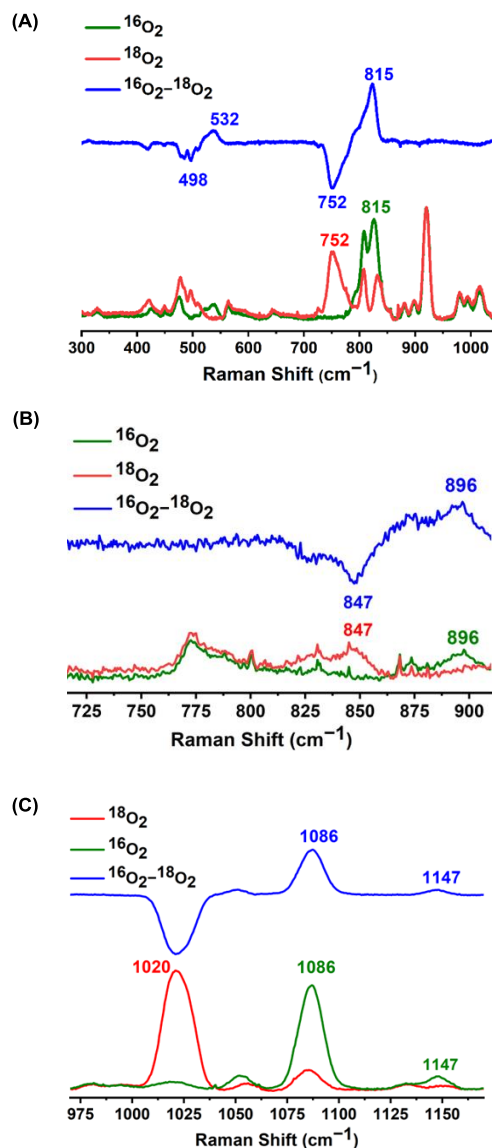
Figure 4. (A) rR spectra in frozen MeTHF solvent (λ_{exc} = 531 nm) of peroxo complex [Cu$^{II}_2$(BPMPO$^-$)(O$_2^{2-}$)]$^{2+}$ using ^{16}O$_2$ (green), ^{18}O$_2$ (red); the difference spectrum (^{16}O$_2$–^{18}O$_2$, blue). (B) rR spectra (λ_{exc} = 380 nm) of [Cu$^{II}_2$(BPMPO$^-$)($^-$OOH)]$^{2+}$ (made by lutidinium triflate protonation of the peroxo precursor, vide supra) using ^{16}O$_2$ (green), ^{18}O$_2$ (red), and the difference spectrum (^{16}O$_2$–^{18}O$_2$, blue) in frozen acetonitrile solvent. (C) rR spectra (λ_{exc} = 407 nm) of superoxo complex [Cu$^{II}_2$(BPMPO$^-$)(O$_2^{\bullet-}$)]$^{2+}$ using ^{16}O$_2$ (green), ^{18}O$_2$ (red); the difference spectrum (^{16}O$_2$–^{18}O$_2$, blue) in frozen MeTHF solvent.[37]

Confirmation that the peroxo-dicopper(II) complex $[Cu^{II}_2(BPMPO^-)(O_2^{2-})]^{1+}$ is generated comes from resonance Raman (rR) spectroscopy (Figure 4A). $[Cu^{II}_2(BPMPO^-)(O_2^{2-})]^{1+}$ rR spectra consist of features around 532 cm^{-1} and 815 cm^{-1}. The band assigned at 815 cm^{-1} is split into two bands, which may be attributed to a Fermi resonance. Using $^{18}O_2$, the 815 cm^{-1} absorption shifts to 752 cm^{-1} ($\Delta(^{18}O_2) = -63$ cm^{-1}). The absolute band position and 18-O shift readily lead these features to be assigned to the peroxide O–O stretch (Figure 4A). The Cu-O stretch region also exhibits an isotope-sensitive feature at 532 cm^{-1}, which shifted by -34 cm^{-1} in the ^{18}O spectrum (Figure 4A). For the hydroperoxo complex $[Cu^{II}_2(BPMPO^-)(^-OOH)]^{2+}$, excitation at 380 nm gave a rR spectrum with an O–O stretch at 896 cm^{-1} (Figure 4B).[37] Since this complex is readily generated using O_2, carrying out an experiment with $^{18}O_2$ was straightforward ($\Delta^{18}O_2 = -49$ cm^{-1}). Laser excitation at 407 nm of a frozen solution of the putative superoxo–dicopper(II) complex gave an intense oxygen isotope-sensitive O–O stretching vibration at 1086 cm^{-1} ($\Delta^{18}O_2 = -66$ cm^{-1}) and a minor component with $v_{O-O} = 1147$ cm^{-1} ($\Delta^{18}O_2 = -61$ cm^{-1}) (Figure 4; bottom) confirming the superoxide designation in $[Cu^{II}_2(BPMPO^-)(O_2^{\bullet-})]^{2+}$. We conclude that two isomers are present, the dominant one having a μ-1,2-$O_2^{\bullet-}$ coordination (consistent with this being the energetically stable isomer in DFT calculations, vide infra), and the other consistent with a μ-1,1-structure (Figure 1), as previously observed for superoxo–dicopper(II) complexes with phenolato binucleating ligands XYLO$^-$ and UNO$^-$ (Figure 5).[20,21b] Further, our DFT calculations (see below and in the SI) suggest that the μ-1,2-superoxo isomer has a lower v_{O-O}. Additionally, two oxygen isotope-sensitive Cu–O stretches are also observed at lower energy (432 cm^{-1}, $\Delta^{18}O_2 = -14$ cm^{-1}; and 529 cm^{-1}, $\Delta^{18}O_2 = -13$ cm^{-1}).[37] This observation of two Cu–O stretches in rR is consistent with the lower symmetry and different Cu–O bond lengths in the DFT calculated structure of $[Cu^{II}_2(BPMPO^-)(O_2^{\bullet-})]^{2+}$ (vide infra).
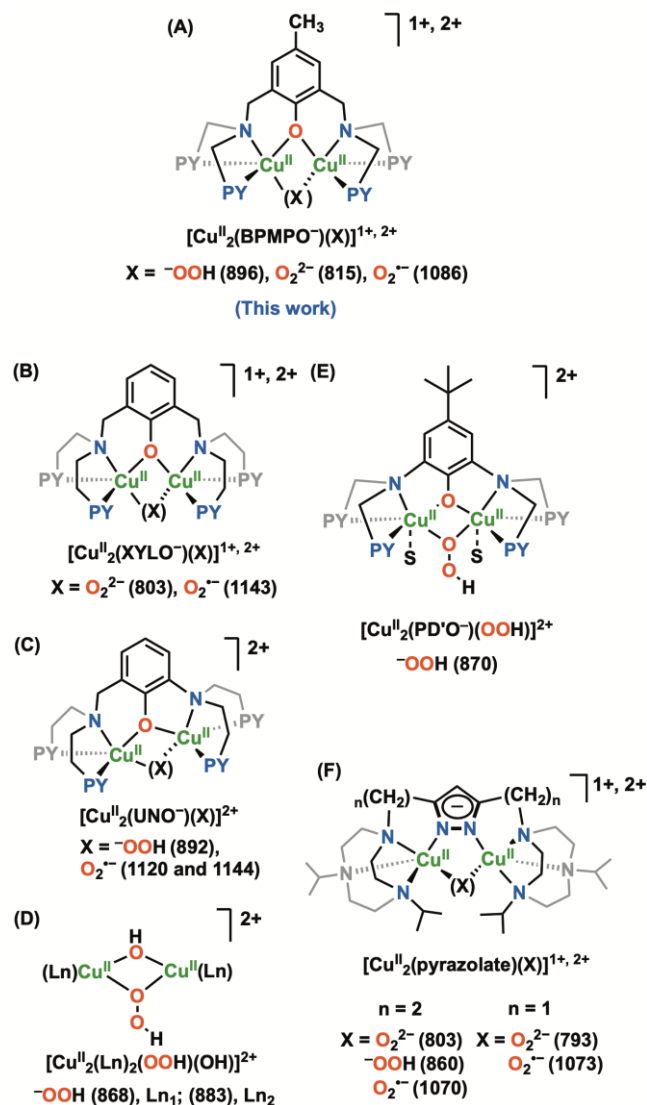
Figure 5. rR spectroscopically derived v(O–O) frequencies (in parentheses; cm^{-1}) for literature peroxide–, hydroperoxide– and superoxide–dicopper(II) complexes, compared to those determined in the present work, for the corresponding complexes with BPMPO$^-$ (A). **S** stands for a solvent molecule and **Ln** stands for either tridentate or tetradentate N$_3$ or N$_4$ chelates. See text for further discussion and references.

Comparisons for the O–O Stretching Frequencies of this Work with Other Related Binuclear Copper Bound Reduced O$_2$ Intermediates. Figure 5 provides the O–O stretching frequencies obtained from rR spectroscopy for the present BPMPO$^-$ containing complexes along with other related dicopper(II) complexes possessing superoxo (μ-1,1 and μ-1,2), μ-1,2-peroxo or μ-1,1-hydroperoxo complexes with different bridging ligands (i.e., a pyrazolato moiety by Meyer *et al.*, a phenolato bridge from our own research and a hydroxide bridge by Suzuki *et al.*(Figure 5)).

The O–O stretch for $[Cu^{II}_2(BPMPO^-)(O_2^{2-})]^{1+}$ peroxo complex is observed at 815 cm^{-1} in rR while that for the structurally related $[Cu^{II}_2(XYLO^-)(O_2^{2-})]^{1+}$ complex is at 803 cm^{-1} (Figure 5B).[18c] Two peroxo dicopper(II) complexes with pyrazolato bridging reported by Meyer *et al.* possess O–O stretching vibrations at 803 (n=2), and 793 cm^{-1} (n=1) (Figure 5F). One may compare these values with those having an end-on coordination with terminal single Cu–O$_{peroxo}$ bonds, but not possessing an internal ligand which bridges two copper ions. These complexes also have O–O stretching frequencies in a similar energy range. The first such example was the *trans-μ-1,2*-peroxo dicopper complex $[\{(TMPA)Cu^{II}\}_2(\mu$-1,2-$O_2^{2-})]^{2+}$ (TMPA = tris(2-pyridylmethyl)amine) with v_{O-O} = 832 cm^{-1}.[38] A number of similar complexes are reported, which employ tripodal N$_4$ or N$_3$S$_{thioether}$ tetradentate chelates for copper ion and their v_{O-O} values are in the range of 811–848 cm^{-1}.[11e]

The other major type of peroxo–dicopper(II) complexes group are the μ-η^2:η^2-peroxo dicopper(II) complexes,[11a,e] with a side-on bridge binding like those in oxy-Hc or oxy-Ty (Scheme 1), and the first synthetic analog with this structure was reported from Fujisawa and Kitajima (v_{O-O} = 741 cm^{-1}).[39] Several other synthetic analogs with such structures (which possess two (2) Cu^{II}–O$_{peroxo}$ bonds for each copper ion) have been subsequently reported. The exceedingly reduced v_{O-O}(peroxo) values (713–773 cm^{-1})[40] arise due to the π-backbonding of copper *d*-orbital into the empty peroxo σ^* orbital.[41]

The rR spectrum of the μ-1,1-hydroperoxo complex $[Cu^{II}_2(BPMPO^-)(^-OOH)]^{2+}$ with O–O stretching vibration at 896 cm^{-1} (Figure 4 top) matches well with that observed for our previously published structurally related phenoxide- and hydroperoxide-bridged complexes: $[Cu^{II}_2(UNO^-)(^-OOH)]^{2+}$ (v_{O-O}) 892 cm^{-1} (Figure 5C)[22a] and is also relatively close to that found for $[Cu^{II}_2(PD'O^-)(^-OOH)]^{2+}$ (v_{O-O}) 870 cm^{-1} (Figure 5E).[22b] As previously observed and as expected, these stretching vibrations occur at a higher energy than those for the corresponding peroxo complexes.[22a] One factor contributing to such a higher v_{O-O} in hydroperoxo complexes is the protonation which withdraws electron density from the peroxo half occupied π^* orbital. These data also compare closely with rR data from two μ-hydroxo-μ-hydroperoxo dicopper(II) species from Suzuki and co-workers[42] (v_{O-O} = 868 cm^{-1}; X-ray structure available) or 883 cm^{-1} (Figure 5D) and the hydroperoxo dicopper(II) complex with additional pyrazolato bridge by Meyer group, v_{O-O} = 860 cm^{-1}) (Figures 1, 5F).[16c] The O–O stretching vibration for monocopper(II) hydroperoxo complexes also falls in the region of 820 to 900 cm^{-1}.[11e]

As discussed, we observed both at 1086 cm^{-1} and 1147 cm^{-1} (Figure 4 bottom) rR bands for $[Cu^{II}_2(BPMPO^-)(O_2^{\bullet-})]^{2+}$, as observed with our previously repored phenolato and superoxo bridged dicopper(II) complexes. For $[Cu^{II}_2(XYLO^-)(O_2^{\bullet-})]^{2+}$ 1143 and 1103 cm^{-1} bands were confirmed as superoxo O–O stretching vibrations[20] while those for $[Cu^{II}_2(UNO^-)(O_2^{\bullet-})]^{2+}$ occur at 1144 and 1120 cm^{-1}

(Figure 5C).[21b] These stretching frequencies are also typical for cupric-superoxo complexes, including Cu^I/O$_{2(g)}$ = 1:1 complexes derived from neutral tetradentate ligands (e.g., TMPA).[14,43] However, overall, Cu^I/O$_{2(g)}$ = 1:1 complexes lead to species having O–O stretching vibrations over a wider range of energies (961–1130 cm^{-1});[11e,43] π-back donation of electron density from a copper(II) orbital to the bound superoxo fragment π^* orbital varies considerably with the nature of ligand and the resulting coordination, i.e., η^1- or η^2. The complexes from Tolman and coworkers[11e,44] possess strongly donating anionic bidentate ligands, giving LCu^I/O$_{2(g)}$ derived products with relatively lower v_{O-O} (961-977 cm^{-1}) and are thus considered to be peroxo-copper(III) complexes.[44] A more recent example is from Itoh and coworkers;[13,44] $[Cu^I(TIPT_3tren)(MeCN)]^+$ which reacts cryogenically with O$_2$ to give a Cu^{III}(η^2-peroxo) complex (v_{O-O}) = 910 cm^{-1}.

It is interesting to note that the rR data for the $[Cu^{II}_2(XYLO^-)(O_2^{\bullet-})]^{2+}$ complex has a characteristic μ-1,2 superoxide O–O stretching vibration at 1143 cm^{-1} as compared to that observed at 1086 cm^{-1} in the newly reported $[Cu^{II}_2(BPMPO^-)(O_2^{\bullet-})]^{2+}$ complex. This decrease in the v(O–O) in $[Cu^{II}_2(BPMPO^-)(O_2^{\bullet-})]^{2+}$ complex correlates with a longer O–O bond length and thus a weaker O–O bond, as observed in DFT optimized structures of these complexes (Figure 6 and Table S4). Further, the O–O bond length obtained from DFT optimized structures of these Cu$^{II}_2$(O$_2^{\bullet-}$) complexes including Meyer *et al.*'s pyrazolate ligand-based complex (Figure 5, n=1) correlate linearly with their experimental O–O stretching frequencies as in a Badger's rule analysis (Figure S11).[37] The geometric structures of the three complexes reveals that the $\angle$Cu–O–O–Cu dihedral angle increases from nearly planar in $[Cu^{II}_2(XYLO^-)(O_2^{\bullet-})]^{2+}$ (~5°) (Figure 6B) to $[Cu^{II}_2(BPMPO^-)(O_2^{\bullet-})]^{2+}$ (~25°) (Figure 6A) to nearly orthogonal in Meyer *et al.*'s pyrazolate ligand-based complex (~84°). A twist of the $\angle$Cu–O–O–Cu dihedral angle from planarity leads to a decrease in the overlap of the filled π^* superoxide orbital with the Cu^{II} LUMOs. This is observed in the analysis of the two Cu^{II} LUMOs. This is observed in the analysis of the two Cu^{II} LUMOs which shows that $[Cu^{II}_2(XYLO^-)(O_2^{\bullet-})]^{2+}$ has the highest filled π^* superoxide orbital donor character (11.7%) followed by $[Cu^{II}_2(BPMPO^-)(O_2^{\bullet-})]^{2+}$ (9.3%) and finally the pyrazolate ligand-based complex (7.0 %) (The two Cu^{II} LUMOs are shown in the SI Figure S20). This increased π-donation out of the in-plane filled antibonding superoxide orbital results in a stronger O–O bond, thus a higher v(O–O) (Table S4).

DFT: BPMPO$^-$ Dicopper(II)–Superoxide Complex, $[Cu^{II}_2(BPMPO^-)(O_2^{\bullet-})]^{2+}$. Meyer's pyrazolato-bridged superoxo-dicopper(II) complex possess only one structural form wherein the O$_2^{\bullet-}$ ligand is bridging in a μ-1,2-fashion (Figure 1). As already noted, two isomers are present for superoxo-dicopper(II) complexes with BPMPO$^-$, XYLO$^-$ and UNO$^-$, the μ-1,2-structure form and the μ-1,1 structure. Our

(A)

1.297 Å

∠(Cu-O-O-Cu) = 25.4°

(B)

1.288 Å

∠(Cu-O-O-Cu) = 4.6°

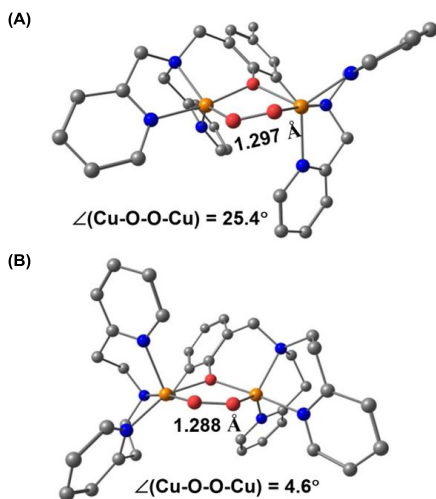**Figure 6**. DFT-optimized geometry for the (A): $[Cu^{II}_2(BPMPO^-)(\mu\text{-}1,2\text{-}O_2^{\bullet-})]^{2+}$, (B) $[Cu^{II}_2(XYLO^-)(O_2^{\bullet-})]^{2+}$, emphasizing calculated superoxo O-O bond distances and ∠Cu–O–O–Cu dihedral angle. See the SI for further details.

DFT calculations reveals that the structure with μ-1,2-binding mode (Figure 6A) is preferred over μ-1,1-binding mode by 6.5 kcal/mol energy, and the $\nu(O–O)$ stretching frequency is relatively higher for the μ-1,1-isomer (Table S5).[37] This finding thus supports the intense peak at 1086 cm^{-1} and weak peak at 1147 cm^{-1} as being associated with the O–O stretch of μ-1,2- and μ-1,1-isomers, respectively. However, the DFT calculation doesn't reproduce the energy difference between the isomers as only the μ-1,2-superoxo isomer should be observed being more stable by 6.5 kcal/mol, while the μ-1,1-superoxo isomer has ~10% intensity in rR with respect to μ-1,2-superoxo isomer. The relative intensity of the vibrations suggests that the μ-1,2-superoxo isomer, $[Cu^{II}_2(BPMPO^-)(O_2^{\bullet-})]^{2+}$, is the primary species present in solution.

EPR Spectroscopy. The EPR spectrum of $[Cu^{II}_2(BPMPO^-)(O_2^{\bullet-})]^{2+}$ at 15 K shows an axial Cu^{II} signal with $g_x = 2.05$, $g_y = 2.01$, $g_z = 2.16$ and $A_x = 6 \times 10^{-4}$ cm^{-1}, $A_y = 2 \times 10^{-4}$ cm^{-1}, $A_z = 53 \times 10^{-4}$ cm^{-1}, as determined from simulation (Figure 7 and 8D). This observation is interesting because for both the phenolato bridged dicopper–superoxide complexes ($[Cu^{II}_2(UNO^-)(O_2^{\bullet-})]^{2+}$ and $[Cu^{II}_2(XYLO^-)(O_2^{\bullet-})]^{2+}$), which are structurally similar to the $[Cu^{II}_2(BPMPO^-)(O_2^{\bullet-})]^{2+}$ complex, a single line spectrum at $g = \sim2.0$ typical of organic radicals (although broadened) is observed (Figure 8A and 8B).[20,21b] These EPR data for the XYLO$^-$ and UNO$^-$ containing superoxo dicopper(II) complexes were explained as originating from the unpaired electron localized on the $O_2^{\bullet-}$ superoxo moiety with antiferromagnetic coupling between the two copper(II) ions of the complexes.[20,21b] The differing observation here for the BPMP binucleating system is that the Cu^{II}–$(O_2^{\bullet-})$–Cu^{II} moiety exhibits a copper(II)-like monomer EPR spectrum. Meyer *et al.* observed and analyzed

such copper(II)-like EPR data for dicopper(II)-superoxide complexes as coming from the unpaired electron at the superoxide moiety being antiferromagnetically coupled to one of the Cu^{II} ions, leaving the remaining spin on the second Cu^{II} (S = ½) center, which is detected by observation of an axial copper(II)-like EPR spectra.
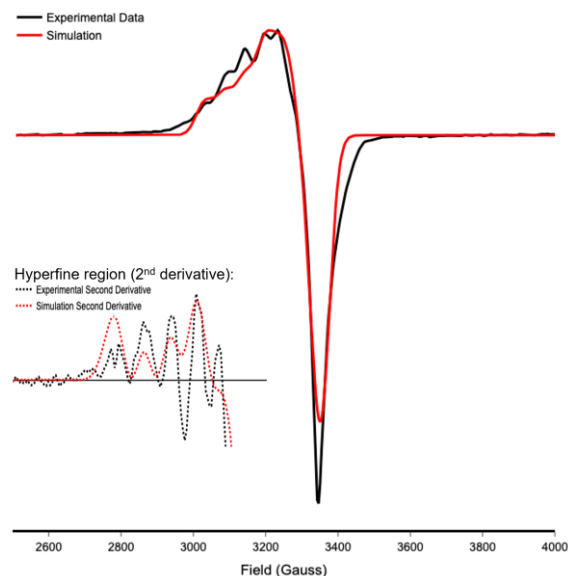
Figure 7. EPR spectrum of $[Cu^{II}_2(BPMPO^-)(O_2^{\bullet-})]^{2+}$ in frozen butyronitrile solution (15 K, X-band) (black line) and the simulated spectrum (red line). The Inset provides comparison of second derivative spectra (dotted lines), focusing on the hyperfine region between 2800 and 3300 Gauss.
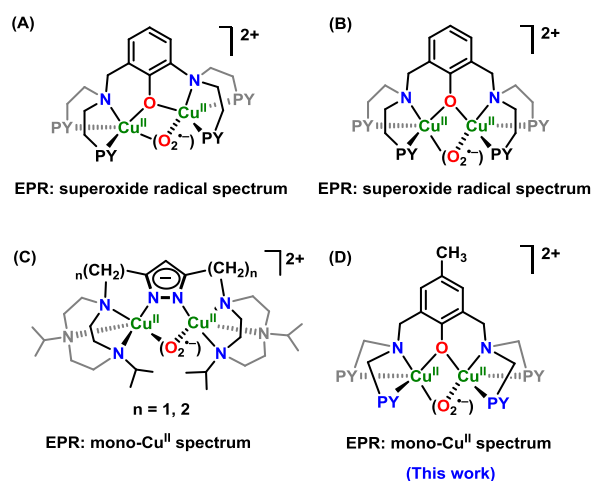
Figure 8. Experimentally derived EPR pattern for previously described superoxo-dicopper(II) complexes (A to C) and for the present case of (D) $[Cu^{II}_2(BPMPO^-)(O_2^{\bullet-})]^{2+}$.

Analysis of the Ground State Wavefunction (Probed by EPR) in the Three-Spin Complexes; $[Cu^{II}_2(XYLO^-)(\mu\text{-}1,2\text{-}O_2^{\bullet-})]^{2+}$, vs $[Cu^{II}_2(BPMPO^-)(\mu\text{-}1,2\text{-}$

$O_2^{\bullet-})]^{2+}$ **vs** $[Cu^{II}_2(\textbf{pyrazolato})(\mu\text{-}1,2\text{-}O_2^{\bullet-})]^{2+}$. The EPR spectrum of the previously reported $[Cu^{II}_2\text{-}$

$(XYLO^-)(O_2^{\bullet-})]^{2+}$ complex shows a single-line superoxide-radical signal ($g = 2.006$; Figure 8B) while the newly reported $[Cu^{II}_2(BPMPO^-)(O_2^{\bullet-})]^{2+}$ complex shows a Cu^{II}-like spectrum ($g_x = 2.01$, $g_y = 2.04$, $g_z = 2.15$; Figure 7) but with a low axial hyperfine coupling $A_z = 78 \times 10^{-4}$ cm^{-1} and a rather low g_z value (2.15) compared to typical mono-Cu(II) complexes corresponding to a delocalized spin with ~50% contribution on Cu^{II}. Such markedly different EPR spectra of these close analogues necessitates an investigation of their electronic structure differences.
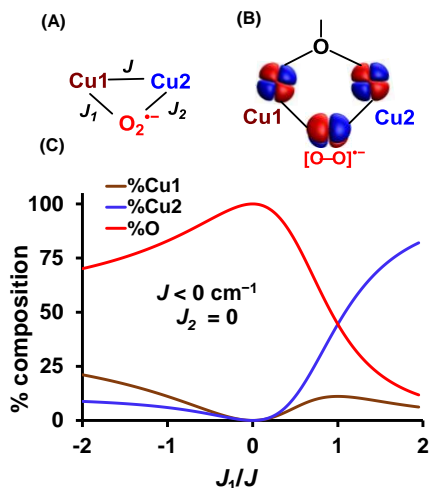
Figure 9. (A) Coupling scheme for $Cu^{II}_2(O_2^{\bullet-})$ complexes with three $S = 1/2$ centers, (B) Schematic representation of magnetic orbitals for the XYLO ligand-based $Cu^{II}_2(O_2^{\bullet-})$ core with Cu_2O_2 in the plane of the paper; $d_{x2\text{-}y2}$ orbital of both Cu's are in the plane of the paper and the π^* $O_2^{\bullet-}$ singly occupied orbital is perpendicular to the plane of the paper and (C) % composition of Cu1 (brown), Cu2 (blue) and $O_2^{\bullet-}$ (red) in the doublet ground state wavefunction for a three-spin $S = 1/2$ system in the linear limit with $J < 0$, $J_1 \neq 0$ and $J_2 = 0$ as per the definitions in Figure 9A.

To obtain insights into the ground state wavefunction of these $Cu^{II}_2(O_2^{\bullet-})$ complexes that gives rise to either a superoxide radical or a Cu^{II}-like EPR signal we employed the three $S = 1/2$ spins exchanged-coupled formalism that was previously applied by our group to study the exchange-coupled Cu^{II} trimer in the oxygen reduction active site in the multicopper oxidases.[45] For an all exchange-coupled three-spin $Cu^{II}_2(O_2^{\bullet-})$ complex as shown in Figure 9A, the spin Hamiltonian is given by:

$$H = -2JS_1.S_2 - 2J_1S_1.S_3 - 2J_2S_2.S_3 \qquad (1)$$

where J denotes the exchange coupling between the two Cu^{II} centers (Cu1 and Cu2) and J_1 and J_2 the exchange coupling between the Cu1 (S_1) and the Cu2 (S_2) with the superoxide (S_3), respectively. The two Cu^{II}s with $S_1 = S_2 = 1/2$ couple to form intermediate spins of $S'_{tot} = 1$ and 0. The

$S'_{tot} = 0$ couples with the superoxide $S_3 = 1/2$ to give the $|1/2, 0\rangle$ state while the $S'_{tot} = 1$ couples to the superoxide $S_3 = 1/2$ to give the $|3/2, 1\rangle$ and the $|1/2, 1\rangle$ states. The $|1/2, 0\rangle$ ground state wavefunction coefficients are given below.

$$c(Cu1) = \tfrac{2}{3}Sin^2\omega + \tfrac{2}{\sqrt{3}}Sin\omega\,Cos\omega \qquad (2)$$

$$c(Cu2) = \tfrac{2}{3}Sin^2\omega - \tfrac{2}{\sqrt{3}}Sin\omega\,Cos\omega \qquad (3)$$

$$c(O_2^{\bullet-}) = Cos^2\omega - \tfrac{1}{3}Sin^2\omega \qquad (4)$$

where ω is given by,

$$\omega = \tfrac{1}{2}tan^{-1}(\tfrac{\sqrt{3}(J_2-J_1)}{2J-J_1-J_2}) \qquad (5)$$

We systematically analyzed all possible combinations of the exchange couplings (J, J_1, J_2) between the three spin centers (Cu1, Cu2 and $O_2^{\bullet-}$) to result in either Cu^{II} or $O_2^{\bullet-}$ character in the ground state wavefunction as probed by EPR (Figure S10).[37] This analysis shows that the necessary condition to have preliminarily Cu^{II}-based wavefunction as observed in $[Cu^{II}_2(BPMPO^-)(O_2^{\bullet-})]^{2+}$ is to have the $O_2^{\bullet-}$ antiferromagnetically coupled with Cu1 with at least the same magnitude as the antiferromagnetic coupling between the Cu's if not higher ($|J_1| \geq |J|$). The third spin (Cu2) can either be coupled with the $O_2^{\bullet-}$ ferromagnetically with a wide range of magnitudes, or antiferromagnetically but with a magnitude similar to the J between the Cu's ($|J_2| \leq |J|$). Alternatively, for the $[Cu^{II}_2(XYLO^-)(O_2^{\bullet-})]^{2+}$ complex, the wavefunction primarily localizes on the $O_2^{\bullet-}$ when Cu1 is ferromagnetically coupled to $O_2^{\bullet-}$ irrespective of the magnitude of J_1 with respect to J and the nature of the coupling of the Cu2 with the $O_2^{\bullet-}$. From DFT calculations, the optimized structure of $[Cu^{II}_2(XYLO^-)(O_2^{\bullet-})]^{2+}$ has the superoxide O–O vector in the plane of the two Cu's ($\angle$Cu–O–O–Cu ~ 5°) (Figure 6B) while $[Cu^{II}_2(BPMPO^-)(O_2^{\bullet-})]^{2+}$ has the superoxide O–O vector rotated out of the equatorial plane of two Cu's ($\angle$Cu–O–O–Cu ~ 25°) (Figure 6A). Therefore, in $[Cu^{II}_2(XYLO^-)(O_2^{\bullet-})]^{2+}$ the $O_2^{\bullet-}$ out-of-plane π^* magnetic orbital is perpendicular to the Cu_2O_2 plane and thus is orthogonal to and thus interacts ferromagnetically with both Cu^{II} magnetic orbitals ($d_{x^2\text{-}y^2}$) that are in the plane of the Cu_2O_2 core (as in Figure 9B). However, in $[Cu^{II}_2(BPMPO^-)(O_2^{\bullet-})]^{2+}$, due to its rotation of the O–O vector out of the plane the $O_2^{\bullet-}$ π^* magnetic orbital would overlap with the magnetic orbital of at least one of the Cu^{II}s leading to an antiferromagnetic interaction that, based on its EPR data would be of similar or greater magnitude than J.

A simple physical picture for the origin of this exchange coupling difference between $[Cu^{II}_2(XYLO^-)(O_2^{\bullet-})]^{2+}$ and $[Cu^{II}_2(BPMPO^-)(O_2^{\bullet-})]^{2+}$ is obtained by considering the limit of a three-spin linear system, i.e., $J_2 = 0$. In this limit when the two Cu^{II}s are antiferromagnetically coupled ($J < 0$), the total spin doublet ground state wavefunction for the three-spin exchanged coupled system is predominant-

ly on the $O_2^{•-}$ when J_1 is ferromagnetic ($J_1/J < 0$ in Figure 9C). The Cu^{II} (Cu2) character starts to build up when J_1 is antiferromagnetic and as it approaches J in magnitude ($J_1/J > 0$ in Figure 9C). *Thus, when the antiferromagnetic interaction between the Cu1 and Cu2 dominates, the wavefunction primarily localizes on the $O_2^{•-}$ and when the antiferromagnetic interaction between the $O_2^{•-}$ and the Cu1 dominates, the wavefunction primarily localizes on Cu2.*

Note that Meyer and co-workers have reported a pyrazolate ligand-based $Cu^{II}_2(O_2^{•-})$ complex which also shows a Cu^{II} EPR signal with similar parameters ($g_x = 2.03$, $g_y = 2.08$, $g_z = 2.15$ and $A_z = 68 \times 10^{-4}$ cm^{-1}) as $[Cu^{II}_2(BPMPO^-)(O_2^{•-})]^{2+}$.[17b] We estimated the exchange coupling between the Cu's (J) for the three $Cu^{II}_2(O_2^{•-})$ complexes using DFT by adding an H-atom to the superoxide center to eliminate the superoxide-radical spin (thus making it a hydroperoxo bridge) without geometry optimization. The J value obtained for the Meyer's complex ($J = -32$ cm^{-1}) is an order of magnitude lower than that calculated for $[Cu^{II}_2(XYLO^-)(O_2^{•-})]^{2+}$ ($J = -687$ cm^{-1}) and $[Cu^{II}_2(BPMPO^-)(O_2^{•-})]^{2+}$ ($J = -267$ cm^{-1}) complexes, reflecting the weaker superexchange pathway between the Cu's via the pyrazolate bridge compared to the phenolate bridge in the $[Cu^{II}_2(XYLO^-)(O_2^{•-})]^{2+}$ and $[Cu^{II}_2(BPMPO^-)(O_2^{•-})]^{2+}$ complexes. Thus, in Meyer's complex the antiferromagnetic coupling of the $O_2^{•-}$ with at least one Cu^{II} could dominate the antiferromagnetic coupling between the Cu's and lead to spin localization on one Cu.

Determination of the Reduction Potential of the $[Cu^{II}_2(BPMPO^-)(O_2^{•-})]^{2+}/[Cu^{II}_2(BPMPO^-)(O_2^{2-})]^{1+}$ Redox Couple. In order to determine the reduction potential for the conversion of superoxide $[Cu^{II}_2(BPMPO^-)(O_2^{•-})]^{2+}$ to peroxide–dicopper(II) $[Cu^{II}_2(BPMPO^-)(O_2^{2-})]^{1+}$ accurately, the reduction of $[Cu^{II}_2(BPMPO^-)(O_2^{•-})]^{2+}$ to $[Cu^{II}_2(BPMPO^-)(O_2^{2-})]^{1+}$ must be a reversible reaction. In fact, we find this to be the case: $[Cu^{II}_2(BPMPO^-)(O_2^{•-})]^{2+}$ and $[Cu^{II}_2(BPMPO^-)(O_2^{2-})]^{1+}$ are interconvertible using redox reagents. Addition of 1.05 equiv. $Cr(\eta^6-C_6H_6)_2$ ($E_{1/2} = -1.15$ V vs Fc$^{+/0}$ in CH$_2$Cl$_2$) to the solution of $[Cu^{II}_2(BPMPO^-)(O_2^{•-})]^{2+}$ resulted in complete reductive conversion of the latter $[Cu^{II}_2(BPMPO^-)(O_2^{2-})]^{1+}$ (Figure 10).
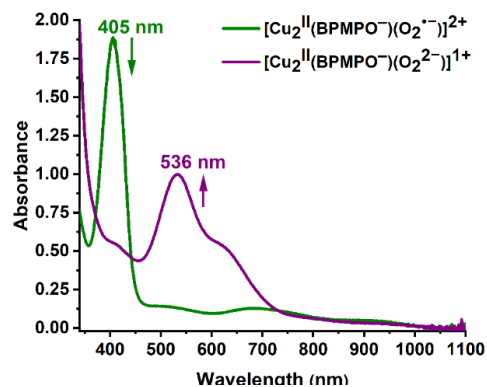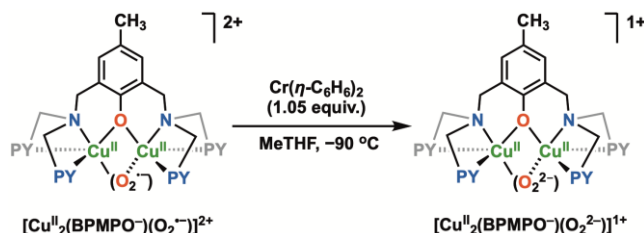
Figure 10. UV–vis spectra illustrating the reduction of $[Cu^{II}_2(BPMPO^-)(O_2^{•-})]^{2+}$ (green) to form $[Cu^{II}_2(BPMPO^-)(O_2^{2-})]^{1+}$ (purple) in MeTHF at –90 °C using $Cr(\eta^6-C_6H_6)_2$.
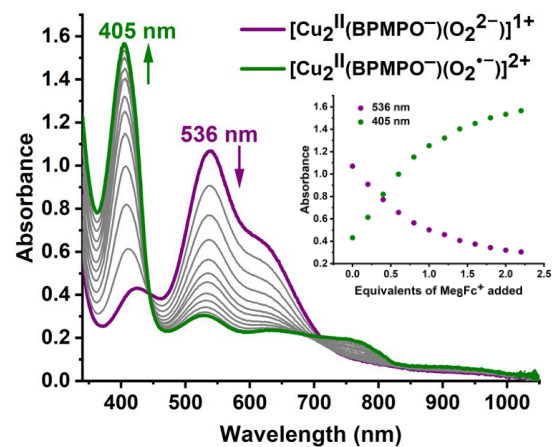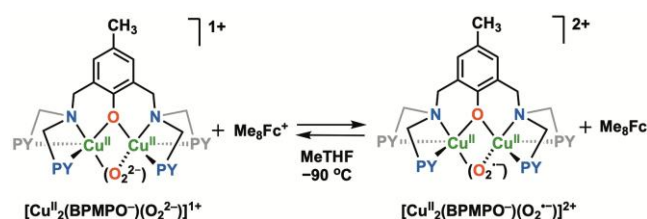
Figure 11. UV–vis spectroscopy monitoring of the incremental addition of 0.2 equiv of Me$_8$Fc$^+$, from 0 to 2.2 equiv, to $[Cu^{II}_2(BPMPO^-)(O_2^{2-})]^{1+}$ in MeTHF at –90 °C resulting in the generation of equilibrium mixtures shown in gray of $[Cu^{II}_2(BPMPO^-)(O_2^{•-})]^{2+}$, Me$_8Fc, Me_8Fc^+$, and $[Cu^{II}_2(BPMPO^-)(O_2^{2-})]^{1+}$ (Table S1),[37] which allowed the determination of the reduction potential of the $[Cu^{II}_2(BPMPO^-)(O_2^{2-})]^{1+}/[Cu^{II}_2(BPMPO^-)(O_2^{•-})]^{2+}$ couple. The low-energy feature at 754 nm is ascribed to Me$_8$Fc$^+$. (Inset) Monitoring of the absorbances at 536 (purple) and 405 (green) nm, demonstrating the decrease and increase of absorbance at the λ_{max} values for $[Cu^{II}_2(BPMPO^-)(O_2^{2-})]^{1+}$ and $[Cu^{II}_2(BPMPO^-)(O_2^{•-})]^{2+}$, respectively.

Interestingly, addition of the octamethylferrocenium (Me$_8$Fc$^+$, $E_{1/2} = -0.43$ V vs Fc$^{+/0}$ in MeTHF),[20,46] to the solution of $[Cu^{II}_2(BPMPO^-)(O_2^{2-})]^{1+}$ leads to the formation of

an equilibrium mixture of dicopper superoxide, and dicopper peroxide, allowing the determination of the reduction potential for the superoxide $[Cu^{II}_2(BPMPO^-)(O_2^{\cdot-})]^{2+}$ /peroxide $[Cu^{II}_2(BPMPO^-)(O_2^{2-})]^{1+}$ couple (Figure 11) by applying the Nernst equation. Titration of varying amounts of Me_8Fc^+ into a MeTHF solution of $[Cu^{II}_2(BPMPO^-)(O_2^{\cdot-})]^{1+}$ at −90 °C resulted in differing concentrations of both $[Cu^{II}_2(BPMPO^-)(O_2^{\cdot-})]^{2+}$ and $[Cu^{II}_2(BPMPO^-)(O_2^{2-})]^{1+}$ in the solution (Figure 11), allowing for the calculation of the equilibrium constant in each concentration (Figure 11 and as described in detail in Table S1). From these equilibrium constants and corresponding calculated $E^{\circ\prime}$ values for each (given the known $E^{\circ\prime}$ of Me_8Fc^+ in MeTHF), the reduction potential of $[Cu^{II}_2(BPMPO^-)(O_2^{\cdot-})]^{2+}$ was calculated to be $E^{\circ\prime}$ = −0.44 ± 0.01 V vs $Fc^{+/\circ}$. Using similar equilibrium measurements generated by various redox reagents, the reduction potential of superoxide–dicopper(II) complex bearing the XYLO⁻ ligand, $[Cu^{II}_2(XYLO^-)(O_2^{\cdot-})]^{2+}$ (Figures 5B, 8B, 10) was previously determined in MeTHF (at −125 °C) to be $E^{\circ\prime}$ = −0.53 ± 0.01 V vs $Fc^{+/\circ}$.[20]

Cryo-electrochemical Study. In order to compare the dicopper(II) superoxo / peroxo reduction potential value obtained by optical titrations (vide supra), electrochemical studies on the *in-situ* generated $[Cu^{II}_2(BPMPO^-)(O_2^{2-})]^{1+}$ complex were performed. As shown in Figure 12, its redox behavior was investigated by cyclic voltammetry (CV) at low temperature (T = 200 K) in acetone/NBu_4PF_6 (0.1 M) with a Pt working electrode. A single reversible system was observed upon oxidation at $E_{1/2}$ = −0.40 V ± 0.01 *vs.* Fc^+/Fc (internal calibration) at scan rate (v) = 0.1 $V.s^{-1}$ in acetone at −73 °C (Figure 12), in rather good agreement with the −0.44 V value obtained by the equilibrium methods described above (MeTHF, −90 °C). The variation of the scan rate from 0.01 V s^{-1} to 0.5 V s^{-1} showed no significant loss of reversibility (Figure S9), hence demonstrating the good stability of the oxidized complex under these conditions.
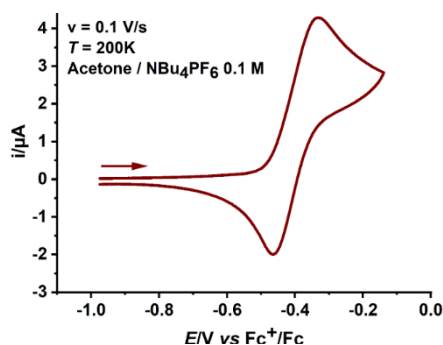
Figure 12. CV (v = 0.1 $V.s^{-1}$) at a Pt working electrode of $[Cu^{II}_2(BPMPO^-)(O_2^{2-})]^{1+}$ (1 mM) in acetone/NBu_4PF_6 (0.1 M); the arrow indicates the scanning direction.

Comparison Redox Potentials. These measured reduction potentials for the superoxide $[Cu^{II}_2(BPMPO^-)(O_2^{\cdot-})]^{2+}$ /peroxide $[Cu^{II}_2(BPMPO^-)(O_2^{2-})]^{1+}$ couple, −0.44 or −0.40 V (vs Fc^+/Fc) are measurably more positive compared to that previously determined for the overall struc-

turally similar phenolato bridged superoxide $[Cu^{II}_2(XYLO^-)(O_2^{\cdot-})]^{2+}$ /peroxide $[Cu^{II}_2(XYLO^-)(O_2^{2-})]^{1+}$ couple, $E^{\circ\prime}$ = −0.53 V in MeTHF at −125 °C (vs Fc^+/Fc). For first thoughts this was somewhat surprising to us, given (as we commented in the Introduction) that we expected redox behavior imparted to the copper ions by the ligand with 5-membered chelate rings (in BPMPO⁻) might have given a clearly more negative potential than for the complex with 6-membered chelate rings (for XYLO⁻). However, the redox is <u>not</u> occurring at the copper ions, but rather just mostly localized on with the dioxygen derived fragment coordinated to the dicopper(II) complexes, the $O_2^{\cdot-}$ or O_2^{2-} bridging ligands. This conclusion was also demonstrated by our analysis and determination of reorganization energy (λ) for the superoxo $[Cu^{II}_2(UNO^-)(O_2^{\cdot-})]^{2+}$ /peroxo $[Cu^{II}_2(UNO^-)(O_2^{2-})]^{1+}$ couple.[21b] As will be explained in the Summary/Conclusion section, we postulate that the more positive superoxo-peroxo redox potential in the BPMPO⁻ compared to XYLO⁻ can be explained by an enhanced Lewis acidity of the Cu(II) ions for the former, the origin of this being due to difference in binding affinity of copper ion for a chelate with five-membered vs six-membered rings.

Another comparison that needs to be made with respect to the reduction potential of the superoxide/peroxide dicopper(II) complexes is to that of the Meyer *et al.*'s pyrazolato-bridged superoxo/peroxo complexes (Figures 5F and 8C; n = 2) with an $E_{1/2}$ = −0.59 V. Our XYLO⁻ ($E^{\circ\prime}$ = −0.53 V) and BPMPO⁻ superoxo/peroxo dicopper(II) complex reduction potentials are more positive, especially that for the BPMPO⁻ ($E^{\circ\prime}$ = −0.44 (or −0.40) V (vs Fc^+/Fc). These differences are significant, even though the redox measurements occur via different techniques (CV vs equilibrium titrations), different organic solvents and varying temperatures. As was previously discussed for the XYLO⁻ case[20] the pyrazolato superoxo-dicopper(II) complex's more negative superoxo-peroxo reduction potential is a major contributor to its ~10 kcal/mol weaker hydroperoxo dicopper(II) OO–H BDFE (vide infra).

Determination of the pK_a Value of $[Cu^{II}_2(BPMPO^-)(^-OOH)]^{2+}$. The p$K_a$ value of the hydroperoxo complex $[Cu^{II}_2(BPMPO^-)(^-OOH)]^{2+}$ has also been evaluated using equilibrium titration method, in MeTHF solution at −90 °C using the derivatized phosphazene base $^tBuP_1(pyrr)$ (pK_a = 22.8 in THF for the conjugate acid at room temperature) to convert varying amounts of $[Cu^{II}_2(BPMPO^-)(^-OOH)]^{2+}$ to the peroxo complex $[Cu^{II}_2(BPMPO^-)(O_2^{2-})]^{1+}$. Using UV–vis spectroscopy, $^tBuP_1(pyrr)$ was added incrementally to $[Cu^{II}_2(BPMPO^-)(^-OOH)]^{2+}$ (Figure 13); the absorption band at 391 nm due to $[Cu^{II}_2(BPMPO^-)(^-OOH)]^{2+}$ decreased with
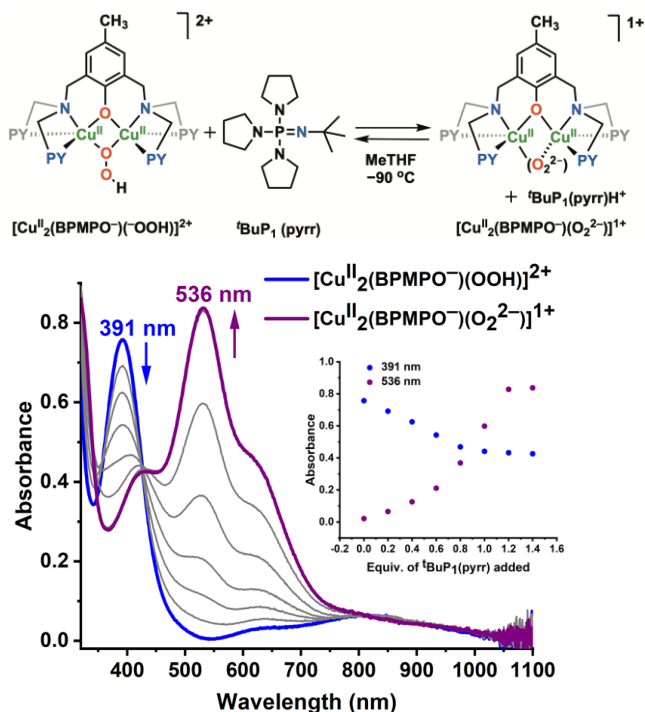
Figure 13. Top: Reaction equation for the hydroperoxo to peroxo deprotonation using the base $^tBuP_1$(pyrr). Middle: UV–vis spectroscopic monitoring of the incremental addition of $^tBuP_1$(pyrr) to a solution of 100% $[Cu^{II}_2(BPMPO^-)(^-OOH)]^{2+}$ (blue spectrum), resulting in the formation of equilibrium mixtures of $[Cu^{II}_2(BPMPO^-)(^-OOH)]^{2+}$, $^tBuP_1$(pyrr), $[Cu^{II}_2(BPMPO^-)(O_2^{2-})]^{1+}$ (purple), and protonated base $^tBuP_1$(pyrr)H$^+$, which allowed the determination of the pK_a value (22.3 ± 0.7) of $[Cu^{II}_2(BPMPO^-)(^-OOH)]^{2+}$. (Inset) monitoring of the absorbance at 391 nm (blue) and 536 nm (purple) during the titration.

increasing concentration of added $^tBuP_1$(pyrr), while a new absorption corresponding to the peroxide complex developed at 536 nm; an isosbestic point was observed at 429 nm, consistent with the direct interconversion of hydroperoxo and peroxo dicopper complexes with formation of the conjugate acid of $^tBuP_1$(pyrr) (Figure 13). Thus, the intermediate spectral curves in Figure 13 (Middle) represent varying equilibrium mixtures. With the known pK_a for $^tBuP_1$(pyrr) in THF (assumed here to be very close to our cryogenically formed solutions in MeTHF), the pK_a value for the deprotonation of $[Cu^{II}_2(BPMPO^-)(^-OOH)]^{2+}$ was determined to be 22.3 ± 0.7 (MeTHF, –90 °C) (see Table S2). This value will be compared to those previously determined for the hydroperoxo-dicopper(II) complex with the XYLO$^-$ ligand (Chart 1, Figures 1, 5), see the discussion below.

Determination of the OO–H BDFE of $[Cu^{II}_2(BPMPO^-)(^-OOH)]^{2+}$. The diagonal relationship of the thermodynamic square scheme (Scheme 2) provides the BDFE representing the reaction where one hydrogen-

atom (H•) is added to the superoxo complex $[Cu^{II}_2(BPMPO^-)(O_2^{\bullet-})]^{2+})$ (Scheme 2). This can be determined utilizing the presently measured fundamental physical properties, (i) the reduction of the superoxo–dicopper(II), $[Cu^{II}_2(BPMPO^-)(O_2^{\bullet-})]^{2+}$ to the peroxo–dicopper(II), $[Cu^{II}_2(BPMPO^-)(O_2^{2-})]^{1+}$ and (ii) the deprotonation of hydroperoxo–dicopper(II), $[Cu^{II}_2(BPMPO^-)(^-OOH)]^{2+}$ to give the peroxo–dicopper(II) compound. The BDFE for the OO–H bond in the complex $[Cu^{II}_2(BPMPO^-)(^-OOH)]^{2+}$ is determined via application of the Bordwell relationship (**eq 6**). When we apply the parameters determined here (vide supra), the reduction potential for the superoxo/peroxo redox couple $E^{o\prime}$ = –0.44 V vs Fc$^{+/o}$, and the pK_a = 22.3 for the $[Cu^{II}_2(BPMPO^-)(^-OOH)]^{2+}$ and with the solvent-dependent term C_G (59.9 kcal/mol for THF, a recently updated value,[23b,c] which is assumed to be essentially the same for the MeTHF solvent used here), the BDFE of the OO–H bond in $[Cu^{II}_2(BPMPO^-)(^-OOH)]^{2+}$ is 80.3 ± 1.2 kcal/mol (**eq 7**). We note that if we input the redox potential obtained from cyclic voltammetry (vide supra), –0.40 V (vs Fc$^+$/Fc) the change in our finally determined OO–H BDFE would be only ~ 1.0 kcal/mole greater (81.3 kcal/mol). The DFT calculated BDFE of $[Cu^{II}_2(BPMPO^-)(^-OOH)]^{2+}$ is 79.4 kcal/mol in agreement with the experimental value.

$$BDFE_{OO-H} = 1.37\ (pK_a) + 23.06(E^{o\prime}(\text{superoxo/peroxo})) + C_G \tag{6}$$

Comparisons for μ-1,1-hydroperoxo OO–H BDFE's. In 2017, the Meyer group[17a] determined the OO–H BDFE of a binuclear copper-hydroperoxide complex possessing a binucleating pyrazolate-bridged ligand framework (Figure 5F & Scheme 4), also by using the thermodynamic square scheme. Their reported hydroperoxo–dicopper(II) OO–H BDFE is 69.4 kcal/mol for acetonitrile solution (a revised value lowered by 2.3 kcal/mol, due to an updated C_G value used here),[23b,c] ~ 11 kcal/mol lower in energy than that was calculated for our XYLO$^-$ containing dicopper–hydroperoxide complex, $[Cu^{II}_2(XYLO^-)(^-OOH)]^{2+}$ (Scheme 4) BDFE = 80.7 kcal/mol for MeTHF solution (also revised due to an updated C_G value for THF). In the present study, we observe the OO–H BDFE for $[Cu^{II}_2(BPMPO^-)(^-OOH)]^{2+}$ of 80.3 kcal/mol, essentially the same as observed for our $[Cu^{II}_2(XYLO^-)(^-OOH)]^{2+}$ system. Thus, while the reduction potential of the new BPMPO$^-$ ligand-based complex is higher than that of the XYLO$^-$ ligand-based complex, a lower pK_a of the former complex compared to the latter complex results in very similar BDFE's for both (Scheme 4). These findings suggest that the superoxo-dicopper(II) complexes with phenolato-bridging ligands and pyridylalkylamine tridentate chelates are considerably stronger oxidants (for hydrogen-atom abstraction reactions) than the superoxo-dicopper(II)

Scheme 4. Comparison of the Thermodynamic Parameters Determined for Pyrazolate-Bridged Dicopper(II) Complexes Reported by Meyer group and the Phenolate-Bridged (XYLO⁻) by Karlin Group and the Present Work. Note the Different Solvents used, MeCN vs MeTHF. The Phenolato-Bridged Superoxo-dicopper(II) Complexes are Significantly Strong Oxidants for HAA Reactions (See the Text).
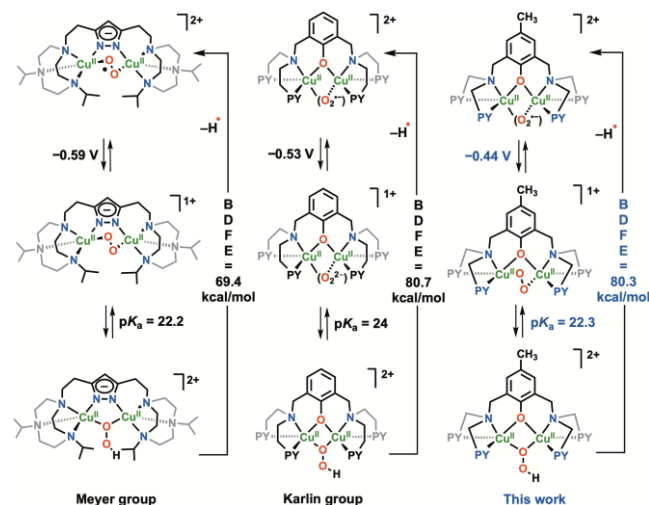
complex that possesses copper ions which are pyrazolato-bridged and triazacyclononane chelated,[17a] since the OO–H bond being formed is much more thermodynamically stable (Scheme 4). Indeed this is the case based on, previously described actual substrate oxidative reactivity comparisons we carried out with $[Cu^{II}_2(XYLO^-)(O_2^{\bullet-})]^{2+}$,[20] and $[Cu^{II}_2(BPMPO^-)(O_2^{\bullet-})]^{2+}$, see below.

We now consider for discussion factors influencing the findings that there are experimentally higher E^o (less negative) and pK_a values for BPMPO⁻ based {Cu₂O₂} congeners in comparison to XYLO⁻systems (vide supra). The net result is that the hydroperoxo dicopper(II) complexes' BDFE are essentially the same.

As for consideration of reduction potential differences, there are surely many factors contributing, such as relative metal ion Lewis acidity (and see below) and coordination geometry differences (which are significant (vide supra). A DFT calculated molecular orbital analysis takes into account all factors (see the SI, Figure S20), revealing a lower energy level of the β-LUMO by 4.3 kcal/mol for the BPMPO⁻ Cu₂-O₂·⁻ complex (–4.123 eV) compared to the corresponding XYLO⁻ complex (–3.936 eV). This suggests the former is more susceptible to reduction. This computational finding correlates with the experimentally observed higher reduction potential for the BPMPO⁻-derived $[Cu^{II}_2(BPMPO^-)(O_2^{\bullet-})]^{2+}$/ $[Cu^{II}_2(BPMPO^-)(O_2^{2-})]^{1+}$ couple (–0.44 V) than for the XYLO⁻ superoxide/peroxide couple (–0.53 V).

Further, related this finding is that it is well established that a stronger Lewis acid binding to a redox active element or group, leads to a more positive redox potential.[47] This further supports that the cupric ions in the BPMPO⁻ complexes are more Lewis acidic than in XYLO⁻ complexes. And this is substantiated based on Cu-O bond lengths

derived from our DFT derived structures. For $[Cu^{II}_2(BPMPO^-)(O_2^{\bullet-})]^{2+}$/ Cu-O$_{superox}$ = 1.961/2.060 Å, while for $[Cu^{II}_2(XYLO^-)(O_2^{\bullet-})]^{2+}$/ Cu-O$_{superox}$ = 2.037/2.078 Å. Also, see the SI, Figure S21. Also, in the complex $[Cu^{II}(TMPA)Cl]^+$ (TMPA, with all 5-membered chelate rings as in BPMPO⁻) vs $[Cu^{II}(TEPA)Cl]^+$ (TEPA, the tripodal N₄ tetradentate analog of TMPA with all six-membered chelate rings as in XYLO⁻), the Cu^{II}-Cl bond distance is shorter in the TMPA complex (2.233 Å vs. 2.289 Å.[48]

This leads to the consideration that the Cu(II) ions in BPMPO⁻-ligated dicopper(II) complexes are more Lewis acidic than in XYLO⁻-bridged Cu₂(II) complexes. Thus, formation of a BPMPO⁻-derived peroxo-dicopper(II) species $[Cu^{II}_2(BPMPO^-)(O_2^{2-})]^{1+}$ by deprotonation of its hydroperoxide conjugate acid $[Cu^{II}_2(BPMPO^-)(^-OOH)]^{2+}$ is expected to be relatively more favorable process than for the case with XYLO⁻. Accordingly, $[Cu^{II}_2(BPMPO^-)(^-OOH)]^{2+}$ would be anticipated to be a stronger acid than $[Cu^{II}_2(XYLO^-)(^-OOH)]^{2+}$, leading to a lower pKa value for the former, as found experimentally, vide supra.

We should comment that OO–H BDFE values for a few other hydroperoxo-metal-complexes (mostly mononuclear; e.g., Co, Fe, Cr, Rh) fall into the range 66-81 kcal/mol, however, the majority of cases have a BDFE in the 70± kcal/mol range.[23c,49] A highly interesting and important case for a copper complexes includes that from Tolman and coworkers;[50] they found that a ligand-Cu^{II}-aqua complexes (where the corresponding Cu^{III}-hydroxide complex effects a HAA reaction) possesses an ~90 kcal/mol BDE (Cu$^{III/II}$, $E^{1/2}$ = –0.074 V vs Fc⁺/Fc), pK_a {Cu^{II}-OH₂} = 18.8). Kieber-Emmons and workers[51] reported that a mono-hydroxo bridged dicopper(II) complex with TMPA chelate, $[(tmpa)Cu^{II}-(OH)-Cu^{II}(tmpa)]^{3+}$, has a BDFE of 103 kcal/mole and pK_a equal to 24.3 in MeCN solvent; by contrast, the mononuclear analog, $[(tmpa)Cu^{II}(OH_2)]^{2+}$ possesses a BDFE of only ~60 kcal/mol (with pK_a = 7.26 in MeCN).

H–atom Abstraction Reactivity Towards TEMPO–H and Substituted Phenols. To further substantiate the HAA reactivity strength of the present superoxo dicopper(II) complex $[Cu^{II}_2(BPMPO^-)(O_2^{\bullet-})]^{2+}$ relative to the BDFE value determined here (BDFE = 80.3 kcal/mol), and relative to the analog $[Cu^{II}_2(XYLO^-)(O_2^{\bullet-})]^{2+}$, we carried out reactions with the substrate TEMPO–H as well as with some representative substituted phenols which are known to undergo HAA reactions producing TEMPO· or ArO· radicals. The reaction of $[Cu^{II}_2(BPMPO^-)(O_2^{\bullet-})]^{2+}$ with TEMPO–H was carried out at –100 °C in MeTHF and monitored by UV-vis spectroscopy (Figure 14). This indeed clearly shows that the hydroperoxo

Figure 14. UV–vis spectra demonstrating the reaction of $[Cu^{II}_2(BPMPO^-)(O_2^{\bullet-})]^{2+}$ at 405 nm (green spectrum) with 20 equiv. of TEMPO–H in MeTHF at –100 °C to yield $[Cu^{II}_2(BPMPO^-)(^-OOH)]^{2+}$ at 391 nm (blue final spectrum). See Supporting Information for the plot of k_{obs} (s–1) vs varying concentrations of TEMPO–H (M) to obtain the second-order rate constant, k_2 = 4.3 ± 0.3 M^{-1} s^{-1}. Yield calculated based on the absorption of $[Cu^{II}_2(BPMPO^-)(^-OOH)]^{2+}$ at 391 nm is 94%. (see Figures S5 & S6 and Table S3 in the Supporting Information for a detailed kinetic study).

complex $[Cu^{II}_2(BPMPO^-)(^-OOH)]^{2+}$ is formed by the completion of the reaction (blue spectrum, Figure 14). Also, TEMPO• was proven to be the other product, based on EPR spectroscopic monitoring (81% yield).[37] Reaction kinetic studies under pseudo first-order conditions (20-50 equiv) were carried out[37] and a plot of k_{obs} *vs* TEMPO–H concentration gives linear behavior; with the second-order rate constant k_2 = 4.3 ± 0.3 M^{-1} s^{-1} (Figure S6 and **eq. 7**). To compare, this k_2 value is 33 times greater than that of reported for $[Cu^{II}_2(pyrazolate)(O_2^{\bullet-})]^{2+}$,[17a] however the latter was carried out in CH_3CN solution at –20 °C (**eq. 8**) compared to the –100 °C conditions for reaction of $[Cu^{II}_2(BPMPO^-)(O_2^{\bullet-})]^{2+}$. The $BPMPO^-$ superoxo dicopper(II) complex is immensely more reactive toward TEMPO–H HAA. This observation falls in line with the more than 10 kcal/mol difference in hydroperoxo OO–H BDFE between $[Cu^{II}_2(BPMPO^-)(^-OOH)]^{2+}$ and the pyrazolato-bridged analog. For a direct comparison, TEMPO–H reactions with our previously studied $[Cu^{II}_2(XYLO^-)(O_2^{\bullet-})]^{2+}$ superoxo complex were carried out. We observed the k_2 for $[Cu^{II}_2(XYLO^-)(O_2^{\bullet-})]^{2+}$ HAA is 5.6 $M^{-1}s^{-1}$ at –100 °C in MeTHF (**eq. 9**) which is 1.30 times greater than that for our analog superoxo complex $[Cu^{II}_2(BPMPO^-)(O_2^{\bullet-})]^{2+}$. This is a quite small difference in rate of reaction with the substrate TEMPO–H, and so in rough agreement with the fact that we find the BDFE for the hydroperoxo dicopper(II) complexes to be almost identical, $[Cu^{II}_2(BPMPO^-)(^-OOH)]^{2+}$ vs $[Cu^{II}_2(XYLO^-)(^-OOH)]^{2+}$, 80.3 (or 81.3, vide supra) vs. 80.7 kcal/mol respectively.

$$[Cu^{II}_2(BPMPO^-)(O_2^{\bullet-})]^{2+} + TEMPO–H \xrightarrow[\substack{-100\ °C \\ k_2 = 4.3\ M^{-1}\ s^{-1}}]{MeTHF} [Cu^{II}_2(BPMPO^-)(^-OOH)]^{2+} + TEMPO^\bullet \quad (7)$$

$$[Cu^{II}_2(pyrazolate)(O_2^{\bullet-})]^{2+} + TEMPO–H \xrightarrow[\substack{-20\ °C \\ k_2 = 0.13\ M^{-1}\ s^{-1}}]{CH_3CN} [Cu^{II}_2(pyrazolate)(^-OOH)]^{2+} + TEMPO^\bullet \quad (8)$$

$$[Cu^{II}_2(XYLO^-)(O_2^{\bullet-})]^{2+} + TEMPO–H \xrightarrow[\substack{-100\ °C \\ k_2 = 5.6\ M^{-1}\ s^{-1}}]{MeTHF} [Cu^{II}_2(XYLO^-)(^-OOH)]^{2+} + TEMPO^\bullet \quad (9)$$

Reaction of either phenolato-bridged superoxo-dicopper(II) complexes with TEMPO-H in fact should be "easy", since the BDFE's for the former are 80-81 kcal/mol where the O–H bond in TEMPO-H has a BDFE = 66.5 kcal/mol (for THF as solvent). To better support the BDFE of the OO–H in our dicopper complex we carried out reactions with substrates that are more difficult to oxidize (by HAA). We find that $[Cu^{II}_2(BPMPO^-)(O_2^{\bullet-})]^{2+}$ is not able to oxidize *p*-methoxyphenol (O–H BDFE = 83.1 kcal/ mol, in THF),[20] in MeTHF solution of $[Cu^{II}_2(BPMPO^-)(O_2^{\bullet-})]^{2+}$ at –100 °C; this is even true for a –80 °C solution. However, at –80 °C, $[Cu^{II}_2(BPMPO^-)(O_2^{\bullet-})]^{2+}$ reacts (slowly) with *p*-OMe-2,6-di-tert-butylphenol, having an O–H BDFE = 75.8 kcal/mol, producing the corresponding phenoxyl radical (EPR, g = 2.002, not shown) (see Supporting Information for the UV-vis spectrum).[37] This of course does not really substantiate our finding of a hydroperoxo-dicopper(II) BDFE of over 80 kcal/mol for the $BPMPO^-$ or $XYLO^-$ complexes. However we note that we previously showed that $[Cu^{II}_2(XYLO^-)(O_2^{\bullet-})]^{2+}$ does react with *p*-OMe-2,6-di-tert-butylphenol at –80 °C (over hours) and it even exhibits slow reactivity with *p*-OMe-phenol (O–H BDFE = 83.1 kcal/mol in THF). Thus, since we showed here that $[Cu^{II}_2(BPMPO^-)(^-OOH)]^{2+}$ and $[Cu^{II}_2(XYLO^-)(^-OOH)]^{2+}$ have essentially the same OO–H BDFE, we can state with some confidence that our findings for the absolute value of these hydroperoxo complex OO–H BDFE's are very reasonable.

SUMMARY/CONCLUSIONS

The synthesis and detailed characterization of dioxygen derived complexes, ligand(s)-Cu_n-(X) (X = $O_2^{\bullet-}$, O_2^{2-}, ^-OOH) has been of considerable ongoing interest in the last 30 years, and continues to challenge synthetic bio-inorganic communities.[11d,11e,44,52] Copper bound peroxo, hydroperoxo and superoxo species occur widely in biochemistry, as mentioned in the introduction for Hc and Ty but also in other copper monooxygenases, amine and galactose oxidases and Cu/Zn superoxide dismutase.[6,53] Hydroperoxo-copper chemistries (as a ligand-copper complex or copper(II) salt with H_2O_2) are also frequently utilized in organic compound oxidations.[4,54] A detailed understanding of the properties, reactivities and thermodynamic interrelationships of these transient intermediates is necessary to advance our knowledge concerning copper (and other metal ions) processing of O_2 in chemistry and biology.

In this report, a new family including cryogenically generated dicopper(II)–peroxide, hydroperoxide and

superoxide complexes with a bridging phenolato BPMPO⁻ ligand were synthesized and characterized. The predominant superoxide complex, is the μ-1,2-O₂·⁻ isomer possesses a Cu(II)-like EPR spectrum, differing from the superoxo centered radical analogues previously studied (with UNO⁻ and XYLO⁻, Figures 5, 8). The analysis of this three-spin system in $[Cu^{II}_2(BPMPO^-)(\mu$-1,2-$O_2^{\cdot-})]^{2+}$ (i.e., the two Cu(II) ions and the superoxide radical anion) indicates that the $O_2^{\cdot-}$ moiety is antiferromagnetically coupled to one of the two Cu(II) ions with a magnitude similar to the antiferromagnetic coupling between the two Cu(II) ions giving rise to a Cu(II)-like EPR spectrum with somewhat decreased g_z and A_z parameters due to coupling over the three spins.

The reduction potential ($E^{o\prime}$) for $[Cu^{II}_2(BPMPO^-)(\mu$-1,2-$O_2^{\cdot-})]^{2+}$ was determined to be –0.44 V (vs Fc⁺/° in MeTHF, –90 °C) while the pK_a of 22.3 (MeTHF, –90 °C) was determined for $[Cu^{II}_2(BPMPO^-)(^-OOH)]^{2+}$. Employing the Bordwell equation, the OO–H BDFE of $[Cu^{II}_2(BPMPO^-)(^-OOH)]^{2+}$ was calculated as 80.3 kcal/mol (eq 7). This BDFE is consistent with the observed HAA chemistry with O–H substrates carried out.

As mentioned in Introduction, the structure and bonding properties in reduced O₂-bound metal complexes are altered with modification of metal ion chelating groups. A number of consequences have been clearly observed here relating to differences or variations in the properties of $[Cu^{II}_2(XYLO^-)(X)]^{1+/2+}$ and $[Cu^{II}_2(BPMPO^-)(X)]^{1+/2+}$ (X = O₂²⁻, ⁻OOH, O₂·⁻):

(1) DFT structural analyses reveal that the individual Cu(II) coordination geometries differ. The ∠Cu–O–O–Cu ~ 25° in $[Cu^{II}_2(BPMPO^-)(\mu$-1,2-$O_2^{\cdot-})]^{2+}$ is significantly distorted from the near planarity observed for $[Cu^{II}_2(XYLO^-)(\mu$-1,2-$O_2^{\cdot-})]^{2+}$ (∠Cu–O–O–Cu ~ 5°) and this causes significant changes in the electronic structural properties of the two complexes as evident by EPR and rR spectroscopies (vide supra). The more out-of-plane ∠Cu–O–O–Cu vector in $[Cu^{II}_2(BPMPO^-)(\mu$-1,2-$O_2^{\cdot-})]^{2+}$ results in:

(a) A weaker J between the Cu(II)'s due to a decreased overlap and thus a less efficient superexchange pathway between the Cu(II)'s via the π_σ* O–O orbital resulting in a higher spin density on the Cu(II) in the ground state wavefunction.

(b) A weaker (lower energy) v(O–O) due to a decreased π donation from the $O_2^{\cdot-}$ π_σ* into the Cu(II) LUMOs.

(2) Prior ligand/metal binding and electrochemistry systematic studies on copper complexes reveal that 5-membered (vs 6-) chelate rings give rise to more stable complexes (greater K_{eq} for ligand-chelate binding to the Cu(II) ion);[55] the Cu(II) ions in $[Cu^{II}_2(BPMPO^-)(X)]^{1+/2+}$ are characteristically more Lewis acidic:

(a) A stronger Lewis acid binding to a redox active element or group, leads to a more positive redox potential.[47] As we determined (vide supra), $E^{o\prime}$ ($E\frac{1}{2}$) for the $[Cu^{II}_2(BPMPO^-)(O_2^{\cdot-})]^{2+}/[Cu^{II}_2(BPMPO^-)(O_2^{2-})]^{1+}$ redox couple becomes <u>more positive</u> by ~ 0. 1 V (vide supra; –0.44 V vs. –0.53 V (for the XYLO⁻ system)).

(b) Stronger/shorter $Cu^{II}(O_2^{\cdot-})$ Cu–O bonds will ensue in the BMPMO⁻ system and lead to a longer and weaker superoxo O–O bond, consistent with the notably large difference in v(O–O) values in $[Cu^{II}_2(BPMPO^-)(O_2^{\cdot-})]^{2+}$ (v(O–O) = 1086 cm⁻¹) vs $[Cu^{II}_2(XYLO^-)(O_2^{\cdot-})]^{2+}$ (v(O–O) = 1143 cm⁻¹).

(c) Cu ion Lewis acidity in BPMPO⁻ complexes contributes to the lower OO–H pK_a, 22.3 for $[Cu^{II}_2(BPMPO^-)(^-OOH)]^{2+}$ (Figure 13, Scheme 4), however 24 for $[Cu^{II}_2(XYLO^-)(^-OOH)]^{2+}$ (Scheme 4);[20] the negative charge that forms when the OO–H group deprotonates is better stabilized.

All of these observations have rationalized our research efforts in utilizing the BPMPO⁻ containing shorter armed chelates in the dicopper complexes in order to further understand fundamental properties including inter-relationships between dioxygen-bound (di)copper intermediates. These results provide important insights into (i) designing a new dicopper/dioxygen system for organic oxidations/oxygenation and ORR in fuel cells and batteries for energy applications, and (ii) the reaction mechanism of O₂-processing copper metalloenzymes in biology. The observations made here encourage the design of new sets of ligands which would lead to superoxide-metal complexes possessing stronger HAA abilities, i.e., having protonated peroxide forms with large(r) OO–H BDFE values.

ASSOCIATED CONTENT

Supporting Information.
Experimental section, Analytical details (UV–vis, rR, CSI-MS, ESI-MS, and EPR spectra), E^o and pK_a calculations, and DFT analysis. This material is available free of charge via the Internet at http://pubs.acs.org.

AUTHOR INFORMATION

Corresponding Author

Edward I. Solomon– *Department of Chemistry, Stanford University, Stanford, California 94305, United States and Stanford Synchrotron Radiation Lightsource, SLAC National Accelerator Laboratory, Menlo Park, California 94025, United States*; orcid.org/0000-0003-0291-3199;
Email: edward.solomon@stanford.edu
Kenneth D. Karlin–*Department of Chemistry, The Johns Hopkins University, Baltimore, Maryland 21218, United States*; orcid.org/0000-0002-5675-7040;
Email: karlin@jhu.edu.

Authors
Pradip Kumar Hota–*Department of Chemistry, The Johns Hopkins University, Baltimore, Maryland 21218, United States*; orcid.org/0000-0002-1502-4879
Anex Jose–*Department of Chemistry, Stanford University, Stanford, California 94305, United States*; orcid.org/0000-0002-4924-7886
Sanjib Panda–*Department of Chemistry, The Johns Hopkins University, Baltimore, Maryland 21218, United States*; orcid.org/0000-0001-6556-8009

Eleanor M. Dunietz–*Department of Chemistry, Stanford University, Stanford, California 94305, United States*; orcid.org/0009-0005-0544-3825

Austin E. Herzog–*Department of Chemistry, The Johns Hopkins University, Baltimore, Maryland 21218, United States*

Laurianne Wojcik–*UMR CNRS 6521, Université de Bretagne Occidentale 6 Avenue Le Gorgeu, CS 93837, 29238 Brest Cedex 3, France*; orcid.org/0000-0002-7897-4142

Nicolas Le Poul–*UMR CNRS 6521, Université de Bretagne Occidentale 6 Avenue Le Gorgeu, CS 93837, 29238 Brest Cedex 3, France*; orcid.org/0000-0002-5915-3760

Catherine Belle–*Université Grenoble-Alpes, CNRS, DCM, UMR 5250, 38058 Grenoble, France*; orcid.org/0000-0002-6656-9174

Author Contributions

The manuscript was written through contributions of all authors. All authors have given approval to the final version of the manuscript.

Funding Sources

Any funds used to support the research of the manuscript should be placed here (per journal style).

Notes

The authors declare no competing financial interest.

ACKNOWLEDGMENT

REFERENCES

(1) (a) Pegis, M. L.; Wise, C. F.; Martin, D. J.; Mayer, J. M. Oxygen Reduction by Homogeneous Molecular Catalysts and Electrocatalysts. *Chem. Rev.* **2018**, *118*, 2340-2391. (b) Mano, N.; de Poulpiquet, A. O₂ Reduction in Enzymatic Biofuel Cells. *Chem. Rev.* **2018**, *118*, 2392-2468.

(2) (a) Karlin, K. D.; Itoh, S. "Copper-Oxygen Chemistry," In *Reactive Intermediates in Chemistry and Biology*; S. E. Rokita, Ed.; John Wiley & Sons, Inc.: Hoboken, 2011(b) Lee, J. Y.; Karlin, K. D. Elaboration of copper–oxygen mediated C–H activation chemistry in consideration of future fuel and feedstock generation. *Curr. Opin. Chem. Biol.* **2015**, *25*, 184-193.

(3) (a) Allen, S. E.; Walvoord, R. R.; Padilla-Salinas, R.; Kozlowski, M. C. Aerobic Copper-Catalyzed Organic Reactions. *Chem. Rev.* **2013**, *113*, 6234-6458. (b) McCann, S. D.; Lumb, J.-P.; Arndtsen, B. A.; Stahl, S. S. Second-Order Biomimicry: In Situ Oxidative Self-Processing Converts Copper(I)/Diamine Precursor into a Highly Active Aerobic Oxidation Catalyst. *ACS Cent. Sci.* **2017**, *3*, 314-321. (c) McCann, S. D.; Stahl, S. S. Copper-Catalyzed Aerobic Oxidations of Organic Molecules: Pathways for Two-Electron Oxidation with a Four-Electron Oxidant and a One-Electron Redox-Active Catalyst. *Acc. Chem. Res.* **2015**, *48*, 1756-1766. (d) Wendlandt, A. E.; Suess, A. M.; Stahl, S. S. Copper-Catalyzed Aerobic Oxidative C–H Functionalizations: Trends and Mechanistic Insights. *Angew. Chem., Int. Ed. Engl.* **2011**, *50*, 11062-11087.

(4) Trammell, R.; Rajabimoghadam, K.; Garcia-Bosch, I. Copper-Promoted Functionalization of Organic Molecules: from Biologically Relevant Cu/O₂ Model Systems to Organometallic Transformations. *Chem. Rev.* **2019**, *119*, 2954-3031.

(5) Marais, L.; Vosloo, H. C. M.; Swarts, A. J. Homogeneous oxidative transformations mediated by copper catalyst systems. *Coord. Chem. Rev.* **2021**, *440*, 213958.

(6) Solomon, E. I.; Heppner, D. E.; Johnston, E. M.; Ginsbach, J. W.; Cirera, J.; Qayyum, M.; Kieber-Emmons, M. T.; Kjaergaard, C. H.; Hadt, R. G.; Tian, L. Copper Active Sites in Biology. *Chem. Rev.* **2014**, *114*, 3659-3853.

(7) Rokhsana, D.; M., S. E.; Brown, D. E.; Dooley, D. M. "Amine Oxidase and Galactose Oxidase," In *Copper-Oxygen Chemistry*; S. Itoh and K. D. Karlin, Ed.; John Wiley & Sons, Inc.: Hoboken, 2011; Vol. 4; pp 53-106.

(8) (a) Magnus, K. A.; Hazes, B.; Ton-That, H.; Bonaventura, C.; Bonaventura, J.; Hol, W. G. J. Crystallographic Analysis of Oxygenated & Deoxygenated States of Arthropod Hemocyanin Shows Unusual Differences. *Proteins: Struct. Funct. Genet.* **1994**, *19*, 302-309. (b) Magnus, K. A.; Ton-That, H.; Carpenter, J. E. Recent Structural Work on the Oxygen Transport Protein Hemocyanin. *Chem. Rev.* **1994**, *94*, 727-735.

(9) Cao, W.; Zhou, X.; McCallum, N. C.; Hu, Z.; Ni, Q. Z.; Kapoor, U.; Heil, C. M.; Cay, K. S.; Zand, T.; Mantanona, A. J.; Jayaraman, A.; Dhinojwala, A.; Deheyn, D. D.; Shawkey, M. D.; Burkart, M. D.; Rinehart, J. D.; Gianneschi, N. C. Unraveling the Structure and Function of Melanin through Synthesis. *J. Am. Chem. Soc.* **2021**, *143*, 2622-2637.

(10) Ginsbach, J. W.; Kieber-Emmons, M. T.; Nomoto, R.; Noguchi, A.; Ohnishi, Y.; Solomon, E. I. Structure/function correlations among coupled binuclear copper proteins through spectroscopic and reactivity studies of NspF. *Proc. Natl. Acad. Sci. U. S. A.* **2012**, *109*, 10793-10797.

(11) (a) Mirica, L. M.; Ottenwaelder, X.; Stack, T. D. P. Structure and Spectroscopy of Copper-Dioxygen Complexes. *Chem. Rev.* **2004**, *104*, 1013-1045. (b) Lewis, E. A.; Tolman, W. B. Reactivity of Dioxygen-Copper Systems. *Chem. Rev.* **2004**, *104*, 1047-1076. (c) Hatcher, L. Q.; Karlin, K. D. Oxidant types in copper-dioxygen chemistry: the ligand coordination defines the Cuₙ-O₂ structure and reactivity. *J. Biol. Inorg. Chem.* **2004**, *9*, 669-683. (d) Quist, D. A.; Diaz, D. E.; Liu, J. J.; Karlin, K. D. Activation of dioxygen by copper metalloproteins and insights from model complexes. *J. Biol. Inorg. Chem.* **2017**, *22*, 253-288. (e) Elwell, C. E.; Gagnon, N. L.; Neisen, B. D.; Dhar, D.; Spaeth, A. D.; Yee, G. M.; Tolman, W. B. Copper–Oxygen Complexes Revisited: Structures, Spectroscopy, and Reactivity. *Chem. Rev.* **2017**, *117*, 2059-2107.

(12) (a) Fujisawa, K.; Tanaka, M.; Morooka, Y.; Kitajima, N. A Monomeric Side-On Superoxocopper(II) Complex - Cu(O₂)(Hb(3-*t*bu-5-*i*Prpz)₃). *J. Am. Chem. Soc.* **1994**, *116*, 12079-12080. (b) Chen, P.; Root, D. E.; Campochiaro, C.; Fujisawa, K.; Solomon, E. I. Spectroscopic and electronic structure studies of the diamagnetic side-on Cu^II-superoxo complex Cu(O₂)[HB(3-R-5-(i)Prpz)₃]: Antiferromagnetic coupling versus covalent delocalization. *J. Am Chem. Soc.* **2003**, *125*, 466-474.

(13) Paria, S.; Morimoto, Y.; Ohta, T.; Okabe, S.; Sugimoto, H.; Ogura, T.; Itoh, S. Copper(I)–Dioxygen Reactivity in the Isolated Cavity of a Nanoscale Molecular Architecture. *Eur. J. Inorg. Chem.* **2018**, *2018*, 1976-1983.

(14) Kim, B.; Karlin, K. D. Ligand–Copper(I) Primary O₂-Adducts: Design, Characterization, and Biological Significance of Cupric–Superoxides. *Acc. Chem. Res.* **2023**, *56*, 2197-2212.

(15) (a) Walli, A.; Dechert, S.; Bauer, M.; Demeshko, S.; Meyer, F. BOX Ligands in Biomimetic Copper-Mediated Dioxygen Activation: A Hemocyanin Model. *Eur. J. Inorg. Chem.* **2014**, *2014*, 4660-4676. (b) Goswami, V. E.; Walli, A.; Forster, M.; Dechert, S.; Demeshko, S.; Holthausen, M. C.; Meyer, F. Acid/base triggered interconversion of μ-η²:η²-peroxido and bis(μ-oxido) dicopper intermediates capped by proton-responsive ligands. *Chem. Sci.* **2017**, *8*, 3031-3037.

(16) (a) Dalle, K. E.; Gruene, T.; Dechert, S.; Demeshko, S.; Meyer, F. Weakly Coupled Biologically Relevant Cu^II₂(μ-η¹:η¹-O₂) cis-Peroxo Adduct that Binds Side-On to Additional Metal Ions. *J.*

Am. Chem. Soc. **2014**, *136*, 7428-7434. (b) Kindermann, N.; Bill, E.; Dechert, S.; Demeshko, S.; Reijerse, E. J.; Meyer, F. A Ferromagnetically Coupled (S=1) Peroxodicopper(II) Complex. *Angew. Chem., Int. Ed. Engl.* **2015**, *54*, 1738-1743. (c) Kindermann, N.; Dechert, S.; Demeshko, S.; Meyer, F. Proton-Induced, Reversible Interconversion of a μ-1,2-Peroxo and a μ-1,1-Hydroperoxo Dicopper(II) Complex. *J. Am. Chem. Soc.* **2015**, *137*, 8002-8005. (d) Lohmiller, T.; Spyra, C.-J.; Dechert, S.; Demeshko, S.; Bill, E.; Schnegg, A.; Meyer, F. Antisymmetric Spin Exchange in a μ-1,2-Peroxodicopper(II) Complex with an Orthogonal Cu–O–O–Cu Arrangement and S = 1 Spin Ground State Characterized by THz-EPR. *JACS Au* **2022**, *2*, 1134-1143.

(17) (a) Kindermann, N.; Günes, C.-J.; Dechert, S.; Meyer, F. Hydrogen Atom Abstraction Thermodynamics of a μ-1,2-Superoxo Dicopper(II) Complex. *J. Am. Chem. Soc.* **2017**, *139*, 9831-9834. (b) Brinkmeier, A.; Schulz, R. A.; Buchhorn, M.; Spyra, C.-J.; Dechert, S.; Demeshko, S.; Krewald, V.; Meyer, F. Structurally Characterized μ-1,2-Peroxo/Superoxo Dicopper(II) Pair. *J. Am. Chem. Soc.* **2021**, *143*, 10361-10366.

(18) (a) Karlin, K. D.; Cruse, R. W.; Gultneh, Y.; Hayes, J. C.; Zubieta, J. Peroxide Coordination to a Dicopper(II) Center. Dioxygen Binding to a Structurally Characterized Phenoxide Bridged Binuclear Copper(I) Complex. *J. Am. Chem. Soc.* **1984**, *106*, 3372-3374. (b) Karlin, K. D.; Gultneh, Y.; Hayes, J. C.; Cruse, R. W.; McKown, J. W.; Hutchinson, J. P.; Zubieta, J. Copper Mediated Hydroxylation of an Arene: Model System for the Action of Copper Monooxygenases and the Structures of a Binuclear Cu(I) Complex and its Oxygenated Product. *J. Am. Chem. Soc.* **1984**, *106*, 2121-2128. (c) Pate, J. E.; Cruse, R. W.; Karlin, K. D.; Solomon, E. I. Vibrational, Electronic and Resonance Raman Spectral Studies of $[Cu_2(XYL-O^-)O_2]^+$, a Copper(II) Peroxide Model Complex of Oxyhemocyanin. *J. Am. Chem. Soc.* **1987**, *109*, 2624-2630. (d) Blackburn, N. J.; Strange, R. W.; Cruse, R. W.; Karlin, K. D. Dioxygen-Copper Reactivity: EXAFS Studies of a Peroxo-Dicopper(II) Complex. *J. Am. Chem. Soc.* **1987**, *109*, 1235-1237. (e) Karlin, K. D.; Ghosh, P.; Cruse, R. W.; Farooq, A.; Gultneh, Y.; Jacobson, R. R.; Blackburn, N. J.; Strange, R. W.; Zubieta, J. Dioxygen-Copper Reactivity: Generation, Characterization and Reactivity of a Hydroperoxo-Dicopper(II) Complex. *J. Am. Chem. Soc* **1988**, *110*, 6769-6780. (f) Cruse, R. W.; Kaderli, S.; Karlin, K. D.; Zuberbühler, A. D. Kinetic and Thermodynamic Studies on the Reaction of O2 with Two Dinuclear Copper(I) Complexes. *J. Am. Chem. Soc.* **1988**, *110*, 6882-6883. (g) Karlin, K. D.; Nasir, M. S.; Cohen, B. I.; Cruse, R. W.; Kaderli, S.; Zuberbühler, A. D. Reversible Dioxygen Binding and Aromatic Hydroxylation in O2-Reactions with Substituted Xylyl Dinuclear Copper(I) Complexes: Syntheses and Low-Temperature Kinetic/Thermodynamic and Spectroscopic Investigations of a Copper Monooxygenase Model System. *J. Am. Chem. Soc.* **1994**, *116*, 1324-1336.

(19) (a) Fukuzumi, S.; Tahsini, L.; Lee, Y.-M.; Ohkubo, K.; Nam, W.; Karlin, K. D. Factors That Control Catalytic Two- versus Four-Electron Reduction of Dioxygen by Copper Complexes. *J. Am. Chem. Soc.* **2012**, *134*, 7025-7035. (b) Das, D.; Lee, Y.-M.; Ohkubo, K.; Nam, W.; Karlin, K. D.; Fukuzumi, S. Acid-Induced Mechanism Change and Overpotential Decrease in Dioxygen Reduction Catalysis with a Dinuclear Copper Complex. *J. Am. Chem. Soc.* **2013**, *135*, 4018-4026.

(20) Quist, D. A.; Ehudin, M. A.; Schaefer, A. W.; Schneider, G. L.; Solomon, E. I.; Karlin, K. D. Ligand Identity-Induced Generation of Enhanced Oxidative Hydrogen Atom Transfer Reactivity for a $Cu^{II}_2(O_2^{\cdot-})$ Complex Driven by Formation of a $Cu^{II}_2(^-OOH)$ Compound with a Strong O–H Bond. *J. Am. Chem. Soc.* **2019**, *141*, 12682-12696.

(21) (a) Mahroof-Tahir, M.; Karlin, K. D. A Dinuclear Mixed-Valence Cu(I)/Cu(II) Complex and Its Reversible Reaction with Dioxygen: Generation of a Superoxodicopper(II) Species. *J. Am. Chem. Soc.* **1992**, *114*, 7599-7601. (b) Cao, R.; Saracini, C.; Ginsbach, J. W.; Kieber-Emmons, M. T.; Siegler, M. A.; Solomon, E. I.; Fukuzumi, S.; Karlin, K. D. Peroxo and Superoxo Moieties Bound to Copper Ion: Electron-Transfer Equilibrium with a Small Reorganization Energy. *J. Am. Chem. Soc.* **2016**, *138*, 7055-7066.

(22) (a) Root, D. E.; Mahroof-Tahir, M.; Karlin, K. D.; Solomon, E. I. Effect of Protonation on Peroxo-Copper Bonding: Spectroscopic and Electronic Structure Study of $[Cu_2(UN-O^-)(OOH)]^{2+}$. *Inorg. Chem.* **1998**, *37*, 4838-4848. (b) Li, L.; Sarjeant, A. A. N.; Vance, M. A.; Zakharov, L. N.; Rheingold, A. L.; Solomon, E. I.; Karlin, K. D. Exogenous nitrile substrate hydroxylation by a new dicopper-hydroperoxide complex. *J. Am. Chem. Soc.* **2005**, *127*, 15360-15361.

(23) (a) Warren, J. J.; Tronic, T. A.; Mayer, J. M. Thermochemistry of Proton-Coupled Electron Transfer Reagents and its Implications. *Chem. Rev.* **2010**, *110*, 6961-7001. (b) Wise, C. F.; Agarwal, R. G.; Mayer, J. M. Determining Proton-Coupled Standard Potentials and X–H Bond Dissociation Free Energies in Nonaqueous Solvents Using Open-Circuit Potential Measurements. *J. Am. Chem. Soc.* **2020**, *142*, 10681-10691. (c) Agarwal, R. G.; Coste, S. C.; Groff, B. D.; Heuer, A. M.; Noh, H.; Parada, G. A.; Wise, C. F.; Nichols, E. M.; Warren, J. J.; Mayer, J. M. Free Energies of Proton-Coupled Electron Transfer Reagents and Their Applications. *Chem. Rev.* **2022**, *122*, 1-49.

(24) Robson, R. Complexes of binucleating ligands I. Two novel binuclear cupric complexes. *Inog. Nucl. Chem. Lett.* **1970**, *6*, 125-128.

(25) Okawa, H.; Kida, S. New template syntheses of some macrocycles capable of forming binuclear metal complexes. *Inog. Nucl. Chem. Lett.* **1971**, *7*, 751-754.

(26) Suzuki, M.; Kanatomi, H.; Murase, I. Synthesis and Properties of Binuclear Cobalt(II) Oxygen Adduct with 2,6-Bis[Bis(2-pyridylmethyl)aminomethyl]-4-methylphenol. *Chem. Lett.* **1981**, 1745-1748.

(27) Suzuki, M.; Ueda, I.; Kanatomi, H.; Murase, I. Molecular Structure of a Binuclear Cobalt Dioxgyen Complex, [Co2(2,6-Bis[Bis(2-pyridylmethyl)aminomethyl]-4-methylphenolato)(benzoato)(dioxygen)-(BF4)2•2H2O. *Chem. Lett.* **1983**, 185-188.

(28) (a) Nishida, Y.; Shimo, H.; Maehara, H.; Kida, S. Crystal-Structures and Magnetic-Properties of Binuclear 5-Co-Ordinate Copper(II) Complexes with a Phenolate Bridge and Their Catalytic Functions in Multielectron Redox Reactions. *J. Chem. Soc. Dalton Trans.* **1985**, 1945-1951. (b) Maloney, J. J.; Glogowski, M.; Rohrbach, D. F.; Urbach, F. L. Structural and Spectroscopic Aspects of a Strained Dicopper Complex with a Tripodal Binucleating Ligand. *Inorg. Chim. Acta* **1987**, *127*, L33-L35. (c) Massoud, S. S.; Junk, T.; Mikuriya, M.; Naka, Y.; Mautner, F. A. Synthesis, structure and magnetic characterization of dinuclear copper(II) complexes of 2,6-bis[bis(pyridine-2-ylmethyl)aminomethy1]-4-methylphenol. *Inorg Chem Commun* **2014**, *50*, 48-50. (d) Orio, M.; Bochot, C.; Dubois, C.; Gellon, G.; Hardré, R.; Jamet, H.; Luneau, D.; Philouze, C.; Réglier, M.; Serratrice, G.; Belle, C. The Versatile Binding Mode of Transition-State Analogue Inhibitors of Tyrosinase towards Dicopper(II) Model Complexes: Experimental and Theoretical Investigations. *Chem. Eur. J.* **2011**, *17*, 13482-13494. (e) Torelli, S.; Belle, C.; Gautier-Luneau, I.; Pierre, J. L.; Saint-Aman, E.; Latour, J. M.; Le Pape, L.; Luneau, D. pH-Controlled Change of the Metal Coordination in a Dicopper(II) Complex of the Ligand H−BPMP: Crystal Structures, Magnetic Properties, and Catecholase Activity. *Inorg. Chem.* **2000**, *39*, 3526-3536. (f) Gennarini, F.; David, R.; Lopez, I.; Le Mest, Y.; Reglier, M.; Belle, C.; Thibon-Pourret, A.; Jamet, H.; Le Poul, N. Influence of Asymmetry on the Redox Properties of Phenoxo- and Hydroxo-Bridged Dicopper Complexes: Spectroelectrochemical and Theoretical Studies. *Inorg. Chem.* **2017**, *56*, 7707-7719.

(29) (a) Zheng, S.; Berto, T. C.; Dahl, E. W.; Hoffman, M. B.; Speelman, A. L.; Lehnert, N. The Functional Model Complex [Fe2(BPMP)(OPr)(NO)2](BPh4)2 Provides Insight into the Mechanism of Flavodiiron NO Reductases. *J. Am. Chem. Soc.* **2013**, *135*, 4902-4905. (b) Van Stappen, C.; Lehnert, N. Mechanism of N–N Bond Formation by Transition Metal–Nitrosyl Complexes: Modeling Flavodiiron Nitric Oxide Reductases. *Inorg. Chem.* **2018**, *57*, 4252-4269. (c) Maeda, Y.; Yamamoto, M.; Hayami, S. Electron transfer rate and structure of [Fe2(bpmp)(ppa)2](BF4)2. *J Radioanal Nucl Ch* **2007**, *272*, 651-656. (d) White, C. J.; Lengel, M. O.; Bracken, A. J.; Kampf, J. W.; Speelman, A. L.; Alp, E. E.; Hu, M. Y.; Zhao, J. Y.; Lehnert, N. Distortion of the [FeNO]2 Core in Flavodiiron Nitric Oxide Reductase Models Inhibits N–N Bond Formation and Promotes

Formation of Unusual Dinitrosyl Iron Complexes: Implications for Catalysis and Reactivity. *J. Am. Chem. Soc.* **2022**, *144*, 3804-3820.

(30) (a) Suzuki, M.; Sugisawa, T.; Uehara, A. Dinuclear Cobalt(II) Complexes Containing 1,3-(or 1,5-)Bis[bis(2-pyridylmethyl)amino]-2-propanolato (or -3-pentanolato): Preparation and Reaction with Molecular Oxygen. *Bull. Chem. Soc. Jpn.* **1990**, *63*, 1115-1120. (b) Kamaal, S.; Gupta, M.; Mishra, R.; Ali, A.; Alarifi, A.; Afzal, M.; Das, R.; Ahmad, M. A Three-Dimensional Pentanuclear Co(II) Coordination Polymer: Structural Topology, Hirshfeld Surface Analysis and Magnetic Properties. *Chemistryselect* **2020**, *5*, 13732-13737.

(31) Magherusan, A. M.; Kal, S.; Nelis, D. N.; Doyle, L. M.; Farquhar, E. R.; Que Jr, L.; McDonald, A. R. A Mn^{II}Mn^{III}-Peroxide Complex Capable of Aldehyde Deformylation. *Angew. Chem., Int. Ed. Engl.* **2019**, *58*, 5718-5722.

(32) Rice, D. R.; de Lourdes Betancourt Mendiola, M.; Murillo-Solano, C.; Checkley, L. A.; Ferdig, M. T.; Pizarro, J. C.; Smith, B. D. Antiplasmodial activity of targeted zinc(II)-dipicolylamine complexes. *Bioorgan. Medicinal Chem.* **2017**, *25*, 2754-2760.

(33) (a) Borovik, A. S.; Papaefthymiou, V.; Taylor, L. F.; Anderson, O. P.; Que, L. Models for iron-oxo proteins. Structures and properties of Fe^{II}Fe^{III}, Zn^{II}Fe^{III}, and Fe^{II}Ga^{III} complexes with (μ-phenoxo)bis(μ-carboxylato)dimetal cores. *J. Am. Chem. Soc.* **1989**, *111*, 6183-6195. (b) Zhang, H.-T.; Guo, Y.-H.; Xiao, Y.; Du, H.-Y.; Zhang, M.-T. Heterobimetallic NiFe Cooperative Molecular Water Oxidation Catalyst. *Angew. Chem., Int. Ed. Engl.* **2023**, *62*, e202218859. (c) Zhang, H.-T.; Xie, F.; Guo, Y.-H.; Xiao, Y.; Zhang, M.-T. Selective Four-Electron Reduction of Oxygen by a Nonheme Heterobimetallic CuFe Complex. *Angew. Chem., Int. Ed. Engl.* **2023**, *62*, e202310775.

(34) Smith, S.; Noble, C.; Palmer, R.; Hanson, G.; Schenk, G.; Gahan, L.; Riley, M. Structural and spectroscopic studies of a model for catechol oxidase. *J. Biol. Inorg. Chem.* **2008**, *13*, 499-510.

(35) Buitrago, E.; Vuillamy, A.; Boumendjel, A.; Yi, W.; Gellon, G.; Hardré, R.; Philouze, C.; Serratrice, G.; Jamet, H.; Réglier, M.; Belle, C. Exploring the Interaction of N/S Compounds with a Dicopper Center: Tyrosinase Inhibition and Model Studies. *Inorg. Chem.* **2014**, *53*, 12848-12858.

(36) (a) Patterson, G. S.; Holm, R. H. Structural and electronic effects on the polarographic half-wave potentials of copper (II) chelate complexes. *Bioinorganic Chemistry* **1975**, *4*, 257-275. (b) Augustin, M. A.; Yandell, J. K.; Addison, J. W.; Karlin, K. D. Rates of Electron Transfer and Redox Potentials of some Copper(II) Thioether Complexes. *Inorg. Chim. Acta* **1981**, *55*, L35-L37. (c) Karlin, K. D.; Yandell, J. K. Redox Behavior of Blue Copper Model Complexes. Redox Potentials and Electron-Transfer Kinetics of Some Copper(II)-Copper(I) Complexes with Nitrogen and Thioether Donors. *Inorg. Chem.* **1984**, *23*, 1184-1188. (d) Rorabacher, D. B. Electron transfer by copper centers. *Chem. Rev.* **2004**, *104*, 651-697.

(37) See Supporting Information.

(38) Baldwin, M. J.; Ross, P. K.; Pate, J. E.; Tyeklár, Z.; Karlin, K. D.; Solomon, E. I. Spectroscopic and Theoretical Studies of an End-On Peroxide-Bridged Coupled Binuclear Copper(II) Model Complex of Relevance to the Active Sites in Hemocyanin and Tyrosinase. *J. Am. Chem. Soc.* **1991**, *113*, 8671-8679.

(39) Kitajima, N.; Fujisawa, K.; Fujimoto, C.; Moro-oka, Y.; Hashimoto, S.; Kitagawa, T.; Toriumi, K.; Tasumi, K.; Nakamura, A. A New Model for Dioxygen Binding in Hemocyanin. Synthesis, Characterization and Molecular Structure of the μ-η^2:η^2 Peroxo Dinuclear Copper(II) Complexes, [Cu(HB(3,5-R$_2$pz)$_3$]$_2$(O$_2$) (R = i-Pr and Ph). *J. Am. Chem. Soc.* **1992**, *114*, 1277-1291.

(40) (a) Lam, B. M. T.; Halfen, J. A.; Young, V. G., Jr.; Hagadorn, J. R.; Holland, P. L.; Lledos, A.; Cucurull-Sanchez, L.; Novoa, J. J.; Alvarez, S.; Tolman, W. B. Ligand Macrocycle Structural Effects on Copper-Dioxygen Reactivity. *Inorg. Chem.* **2000**, *39*, 4059-4072. (b) Adam, S. M.; Wijeratne, G. B.; Rogler, P. J.; Diaz, D. E.; Quist, D. A.; Liu, J. J.; Karlin, K. D. Synthetic Fe/Cu Complexes: Toward Understanding Heme-Copper Oxidase Structure and Function. *Chem. Rev.* **2018**, *118*, 10840-11022.

(41) (a) Ross, P. K.; Solomon, E. I. An electronic structural comparison of copper-peroxide complexes of relevance to hemocyanin and tyrosinase active sites. *J. Am. Chem. Soc.* **1991**, *113*, 3246-3259. (b) Park, G. Y.; Qayyum, M. F.; Woertink, J.; Hodgson, K. O.; Hedman, B.; Narducci Sarjeant, A. A.; Solomon, E. I.; Karlin, K. D. Geometric and Electronic Structure of [{Cu(MeAN)}$_2$(μ-η^2:η^2(O$_2$$^{2-}$))]$^{2+}$ with an Unusually Long O–O Bond: O–O Bond Weakening vs Activation for Reductive Cleavage. *J. Am. Chem. Soc.* **2012**, *134*, 8513-8524.

(42) Itoh, K.; Hayashi, H.; Furutachi, H.; Matsumoto, T.; Nagatomo, S.; Tosha, T.; Terada, S.; Fujinami, S.; Suzuki, M.; Kitagawa, T. Synthesis and reactivity of a (mu-1,1-hydroperoxo)(mu-hydroxo)dicopper(II) complex: Ligand hydroxylation by a bridging hydroperoxo ligand. *J. Am. Chem. Soc.* **2005**, *127*, 5212-5223.

(43) Liu, J. J.; Diaz, D. E.; Quist, D. A.; Karlin, K. D. Copper(I)-Dioxygen Adducts and Copper Enzyme Mechanisms. *Isr. J. Chem.* **2016**, *56*, 738-755.

(44) Jeong, D.; Selverstone Valentine, J.; Cho, J. Bio-inspired mononuclear nonheme metal peroxo complexes: Synthesis, structures and mechanistic studies toward understanding enzymatic reactions. *Coord. Chem. Rev.* **2023**, *480*, 215021.

(45) (a) Cole, J. L.; Clark, P. A.; Solomon, E. I. Spectroscopic and chemical studies of the laccase trinuclear copper active site: geometric and electronic structure. *J. Am. Chem. Soc.* **1990**, *112*, 9534-9548. (b) Lee, S.-K.; DeBeer George, S.; Antholine, W. E.; Hedman, B.; Hodgson, K. O.; Solomon, E. I. Nature of the Intermediate Formed in the Reduction of O$_2$ to H$_2$O at the Trinuclear Copper Cluster Active Site in Native Laccase. *J. Am. Chem. Soc.* **2002**, *124*, 6180-6193.

(46) Reduction potentials and pKa values of the reference compounds used in this work come from room temperature literature values. For this study and others, (also see references 20 and 21b) with experiments carried out under cryogenic conditions, we have assumed that temperature dependencies are not so large, however, *E*°' or p*K*a values calculated by utilizing these literature values may have a further uncertainly associated with them.

(47) (a) Yan Poon, P. C.; Dedushko, M. A.; Sun, X.; Yang, G.; Toledo, S.; Hayes, E. C.; Johansen, A.; Piquette, M. C.; Rees, J. A.; Stoll, S.; Rybak-Akimova, E.; Kovacs, J. A. How Metal Ion Lewis Acidity and Steric Properties Influence the Barrier to Dioxygen Binding, Peroxo O–O Bond Cleavage, and Reactivity. *J. Am. Chem. Soc.* **2019**, *141*, 15046-15057. (b) Itoh, S.; Kumei, H.; Nagatomo, S.; Kitagawa, T.; Fukuzumi, S. Effects of Metal Ions on Physicochemical Properties and Redox Reactivity of Phenolates and Phenoxyl Radicals: Mechanistic Insight into Hydrogen Atom Abstraction by Phenoxyl Radical-Metal Complexes. *J. Am. Chem. Soc.* **2001**, *123*, 2165-2175. (c) Tsui, E. Y.; Agapie, T. Reduction potentials of heterometallic manganese–oxido cubane complexes modulated by redox-inactive metals. *Proc. Natl. Acad. Sci. U. S. A.* **2013**, *110*, 10084-10088. (d) Neu, H. M.; Baglia, R. A.; Goldberg, D. P. A Balancing Act: Stability versus Reactivity of Mn(O) Complexes. *Acc. Chem. Res.* **2015**, *48*, 2754-2764. (e) Xue, S.-S.; Li, X.-X.; Lee, Y.-M.; Seo, M. S.; Kim, Y.; Yanagisawa, S.; Kubo, M.; Jeon, Y.-K.; Kim, W.-S.; Sarangi, R.; Kim, S. H.; Fukuzumi, S.; Nam, W. Enhanced Redox Reactivity of a Nonheme Iron(V)–Oxo Complex Binding Proton. *J. Am. Chem. Soc.* **2020**, *142*, 15305-15319.

(48) Karlin, K. D.; Hayes, J. C.; Shi, J.; Hutchinson, J. P.; Zubieta, J. Tetragonal vs. Trigonal Coordination in Copper(II) Complexes with Tripod Ligands: Structures and Properties of (Cu(C$_{21}$H$_{24}$N$_4$)Cl)PF6 and (Cu(C$_{18}$H$_{18}$N$_4$)Cl)PF$_6$. *Inorg. Chem.* **1982**, *21*, 4106-4108.

(49) (a) Gordon, J. B.; Vilbert, A. C.; Siegler, M. A.; Lancaster, K. M.; Moënne-Loccoz, P.; Goldberg, D. P. A Nonheme Thiolate-Ligated Cobalt Superoxo Complex: Synthesis and Spectroscopic Characterization, Computational Studies, and Hydrogen Atom Abstraction Reactivity. *J. Am. Chem. Soc.* **2019**, *141*, 3641-3653. (b) Mondal, P.; Ishigami, I.; Gérard, E. F.; Lim, C.; Yeh, S.-R.; de Visser, S. P.; Wijeratne, G. B. Proton-coupled electron transfer reactivities of electronically divergent heme superoxide intermediates: a kinetic, thermodynamic, and theoretical study. *Chem. Sci.* **2021**, *12*, 8872-8883.

(50) Dhar, D.; Yee, G. M.; Spaeth, A. D.; Boyce, D. W.; Zhang, H.; Dereli, B.; Cramer, C. J.; Tolman, W. B. Perturbing the Copper(III)–Hydroxide Unit through Ligand Structural Variation. *J. Am. Chem. Soc.* **2016**, *138*, 356-368.

(51) VanNatta, P. E.; Ramirez, D. A.; Velarde, A. R.; Ali, G.; Kieber-Emmons, M. T. Exceptionally High O–H Bond Dissociation Free Energy of a Dicopper(II) μ-Hydroxo Complex and Insights into the Geometric and Electronic Structure Origins Thereof. *J. Am. Chem. Soc.* **2020**, *142*, 16292-16312.

(52) Karlin, K. D.; Hota, P. K.; Kim, B. Concluding remarks: discussion on natural and artificial enzymes including synthetic models. *Faraday Discuss* **2022**, *234*, 388-404.

(53) (a) Shepard, E. M.; Dooley, D. M. Inhibition and Oxygen Activation in Copper Amine Oxidases. *Acc. Chem. Res.* **2015**, *48*, 1218-1226. (b) Cowley, R. E.; Cirera, J.; Qayyum, M. F.; Rokhsana, D.; Hedman, B.; Hodgson, K. O.; Dooley, D. M.; Solomon, E. I. Structure of the Reduced Copper Active Site in Preprocessed Galactose Oxidase: Ligand Tuning for One-Electron O2 Activation in Cofactor Biogenesis. *J. Am. Chem. Soc.* **2016**, *138*, 13219-13229. (c) Sheng, Y.; Abreu, I. A.; Cabelli, D. E.; Maroney, M. J.; Miller, A.-F.; Teixeira, M.; Valentine, J. S. Superoxide Dismutases and Superoxide Reductases. *Chem. Rev.* **2014**, *114*, 3854-3918.

(54) (a) Trammell, R.; Cordova, A.; Zhang, S.; Goswami, S.; Murata, R.; Siegler, M. A.; Garcia-Bosch, I.; Trammell, R.; Cordova, A.; Zhang, S.; Goswami, S.; Murata, R.; Siegler, M. A.; Garcia-Bosch, I. Practical One-Pot Multistep Synthesis of 2H-1,3-Benzoxazines Using Copper, Hydrogen Peroxide, and Triethylamine. *Eur. J. Org. Chem.* **2021**, *2021*, 4536-4540. (b) Gogoi, G.; Nath, J. K.; Hoque, N.; Biswas, S.; Gour, N. K.; Kalita, D. J.; Bora, S. R.; Bania, K. K. Single and multiple site Cu(II) catalysts for benzyl alcohol and catechol oxidation reactions. *Applied Catalysis A: General* **2022**, *644*, 118816.

(55) (a) Irving, H.; Williams, R. J. P.; Ferrett, D. J.; Williams, A. E. The influence of ring size upon the stability of metal chelates. *J. Chem. Soc. (Resumed)* **1954**, 3494-3504. (b) Gillard, R. D.; Irving, H. M. Conformational Aspects of Chelate Rings. *Chem. Rev.* **1965**, *65*, 603-616. (c) Heims, F.; Mereacre, V.; Ciancetta, A.; Mebs, S.; Powell, A. K.; Greco, C.; Ray, K. Synthesis and Spectroscopic Characterisation of a Heterodinuclear Iron(III)-Copper(II) Complex Based on an Asymmetric Dinucleating Ligand System. *Eur. J. Inorg. Chem.* **2012**, *2012*, 4565-4569.

Insert Table of Contents artwork here

$E^{o'}$ by (1) Optical redox titration (2) Cryo-electrochemistry